Frequency Ratio Density, Logistic Regression and Weights of Evidence Modelling for Landslide Susceptibility Assessment and Mapping in Yanase and Naka Catchments of Southeast Shikoku, Japan

Matebie Meten (matebe21@gmail.com)
Addis Ababa University College of Social Sciences https://orcid.org/0000-0002-1529-190X
Netra Prakash Bhandary
Ehime University

Research

Keywords: Landslide Susceptibility, Frequency Ratio Density, Logistic Regression, Weights of Evidence, GIS, Japan

Posted Date: August 11th, 2020

DOI: https://doi.org/10.21203/rs.3.rs-37349/v2

Frequency Ratio Density, Logistic Regression and Weights of Evidence Modelling for Landslide Susceptibility Assessment and Mapping in Yanase and Naka Catchments of Southeast Shikoku, Japan

Matebie Meten (PhD)[1*]

Department of Geology

College of Applied Sciences,

Addis Ababa Science and Technology University, Ethiopia

Telephone: +251-911899279

P.O.Box: 16417

E-mail: matebe21@gmail.com

Netra Prakash Bhandary, Ph.D. Eng.(Professor) [2]

Department of Environmental Design, Faculty of Collaborative Regional Innovation

Graduate School of Science and Engineering

Ehime University

3 Bunkyo-cho, Matsuyama 790-8577, JAPAN

Tel/Fax: +81 (0)89 927 8566; Cell: +81 (0)90 3785 5836

Email: netra@ehime-u.ac.jp

Abstract

Landslide susceptibility assessment is an important tool for disaster management and development activities. Shikoku Island in the southwest Japan is one of the most landslide prone areas due to heavy typhoon rainfall, complex geology and the presence of mountainous areas and low topographic features (valleys).Yanase and Naka Catchments of Shikoku Island in Japan were chosen as a study area. The objective of this study is to apply Frequency Ratio Densisty (FRD), Logistic Regression (LR) and Weights of Evidence (WoE) models in a GIS environment to prepare the landslide susceptibility maps of this area and select the best one for future infrastructure and landuse planning. Data layers including slope, aspect, profile curvature, plan curvature, lithology, land use, distance from river, distance from fault and annual rainfall were used in this study. In FR method, two models were attempted but the FRD model was found slightly better in its performance. In case of LR method, two models, one with equal proportion and the other with unequal proportion of landslide and non-landslide points were applied and the one with equal proportions was chosen based on its highest performance. A total of five landslide susceptibility maps(LSMs) were produced using FR, LR and WoE models resulting two, two and one LSMs respectively. However, one best model was chosen from the FR and LR methods based on the highest area under the curve (AUC) of the receiver operating characteristic (ROC) curves. This reduced the total number of landslide susceptibility maps to three with the success rates of 86.7%, 86.8% and 80.7% from FRD, LR and WoE models respectively. For validation purpose, all landslides were overlaid over the three landslide susceptibility maps and the percentage of landslides in each susceptibility class was calculated. The percentages of landslides that fall in the high and very high susceptibility classes of FRD, LR and WoE models showed 82%, 84% and 78% respectively. This showed that the LR model with equal proportions of landslides and non-landslide points was slightly better than FRD and WoE models in predicting the probability of future landslide occurrence.

Key Words

Landslide Susceptibility, Frequency Ratio Density, Logistic Regression, Weights of Evidence, GIS, Yanase and Naka Catchments, Shikoku, Japan

1. Introduction

The Japan archipelago is situated within one of the most active tectonic belts where four major plates interact i.e. the Pacific Plate, the Eurasian Plate, the Philippine Sea Plate and the North American Plate. Hence, most of the Japan landmass is highly susceptible to different natural disasters like landslides, debris- and mudflows due to steep mountains, weak geology and severe weather conditions (Hong et al. 2005). More than 80% of Shikoku Island consists of steep mountain slopes which has a few plain areas along the coastal lines and elevated peaks in the central part.. It is a heavily forested mountainous region of Japan with a mean annual precipitation of range from 1,000mm to 3,500mm (Dahal et al. 2008a). The presence of dense population at the bases of mountains exacerbated the landslide problem. Owing to the geological and morphological settings, landslides and floods caused by typhoon rainfall are frequent. In 2004, Shikoku experienced extreme events of typhoon rainfall andfaced huge losses of life and property. From 1951 to 2005, there were 1468 typhoon events in the northern part of the Pacific Ocean, 163 of which hit the Japanese archipelago. In 2004, Japan was hit by 10 annual typhoon events which were maximumwithin the last 55 years (Dahal et al. 2008a). The isohyetal map of Shikoku showed that the island usually gets more extensive typhoon rainfall in its southernpart than in its northern part.

Landslide susceptibility refers to a quantitative or qualitative assessment of landslides which exist or may potentially occur in an area without taking into account the time of landsliding (Fell et al. 2008). Susceptibility, hazard and risk maps are important tools for engineers, earth scientists, planners and decision makers to select appropriate sites for agriculture, construction and other developmental activities (Ercanoglu and Gokceoglu 2002). They also play an important role in efforts to mitigate or prevent the disaster in landslide prone areas by providing preliminary information to decision makers.

Landslide susceptibility methods can be categorized into heuristic (Ruff and Czurda 2008), deterministic (Gerscovich et al. 2006), combination of statistical and deterministic (Yilmaz and Keskin 2009) and statistical methods.

Statistical methods are further classified into frequency ratio (Lee et al. 2004; Meten et al. 2015a), logistic regression (Ayalew and Yamagishi 2005), artificial neural network (Pradhan et al. 2010), weights of evidence (Dahal et al. 2008b), fuzzy logic (Regmi et al. 2010a), analytical hierarchical process (Ayalew et al. 2004), infoval (Saha et al. 2005), likelihood ratio (Chung 2006), bivariate statistics (Thiery et al. 2007), multivariate statistics (Akgun and Turk 2011), conditional probability (Clerici et al. 2006), multi-criteria analysis (Abella and Van Westen 2008), spatial decision support (Wan 2009), overlay analysis (Ayenew and Barbieri 2005) and combination of the above statistical methods (Ayalew et al. 2005; Meten et al. 2015b).

In heuristic methods, field observation and expert's knowledge are used to identify landslides, make a prior assumption about past and future landslide movements in the site and develop decision rules or assign weighted values for the classes of index maps and overlay them to develop a landslide susceptibility map. Deterministic method considers angle of the slope, strength of slope material (cohesion and internal angle of friction), structure (rock discontinuities, rock and soil stratification), moisture content, depth of groundwater table and pore-water pressure of the slope material in a physical model equation to determine factor of safety (Regmi et al. 2010a). A significant limitation of deterministic models is the need for geotechnical data (cohesion, internal angle of friction, depth to groundwater table, degree of saturation, etc.,) which are difficult to obtain over large areas (Terlien et al. 1995). Moreover, they do not take into

account the climatic and human-induced factors, spatial distribution, temporal frequencies and magnitude of landslides. These methods only provide the stability of the slope during a time of data collection (Regmi et al. 2010a) and may work well for site specific conditions.

The statistical approach, which predicts future landslides based on past landslides (Ohlmacher and Davis 2003), on the other hand can be applied when geotechnical data limitation is a problem. Researches done on landslide susceptibility comparisons using both statistical and deterministic models have shown that the former gives a better result than the latter (Cervi et al. 2010; Yilmaz and Keskin 2009). The current study used the three statistical models of frequency ratio, logistic regression and weights of evidence to prepare the landslide susceptibility maps of the study area and the best model was selected. In the first two models, two alternative models were attempted in order to choose the best one while in the third model only one attempt was made. Then the first two best model outputs were compared with that of the weights of evidence modeling in order to choose the best predictive model among the three approaches.

2. The Study Area

The study area is located in Tokushima and Kochi prefectures of Shikoku Island, Southwest Japan covering an area of 599.724 Km^2 in atopographically rugged and mountainous terrain with an elevation range lying between 205m and 1950 m above sea level (Fig. **1**). This area is bounded between 33˚35” N and 33˚55” N latitude and 134˚1” E and 134˚21” E longitude containing the highest mountain chains in Shikoku Island including Mt. Tsurugi, Mt. Takashiro, Mt. Ishidate, Mt. Akagio, Mt. Nishimata, Mt. Hozo, Mt. Kamedani, Mt. Goya, Mt. Tani, Mt. Kuwanoki and Mt. Ikenoko with associated steep slopes (Fig. **1**). Besides,the study area is located in the southeastern part of Shikoku island, particularly in the Yanase - Tsurugisan - Kito rainfall belt where maximum rainfall is prevailing (Fig. **2 and 3**).

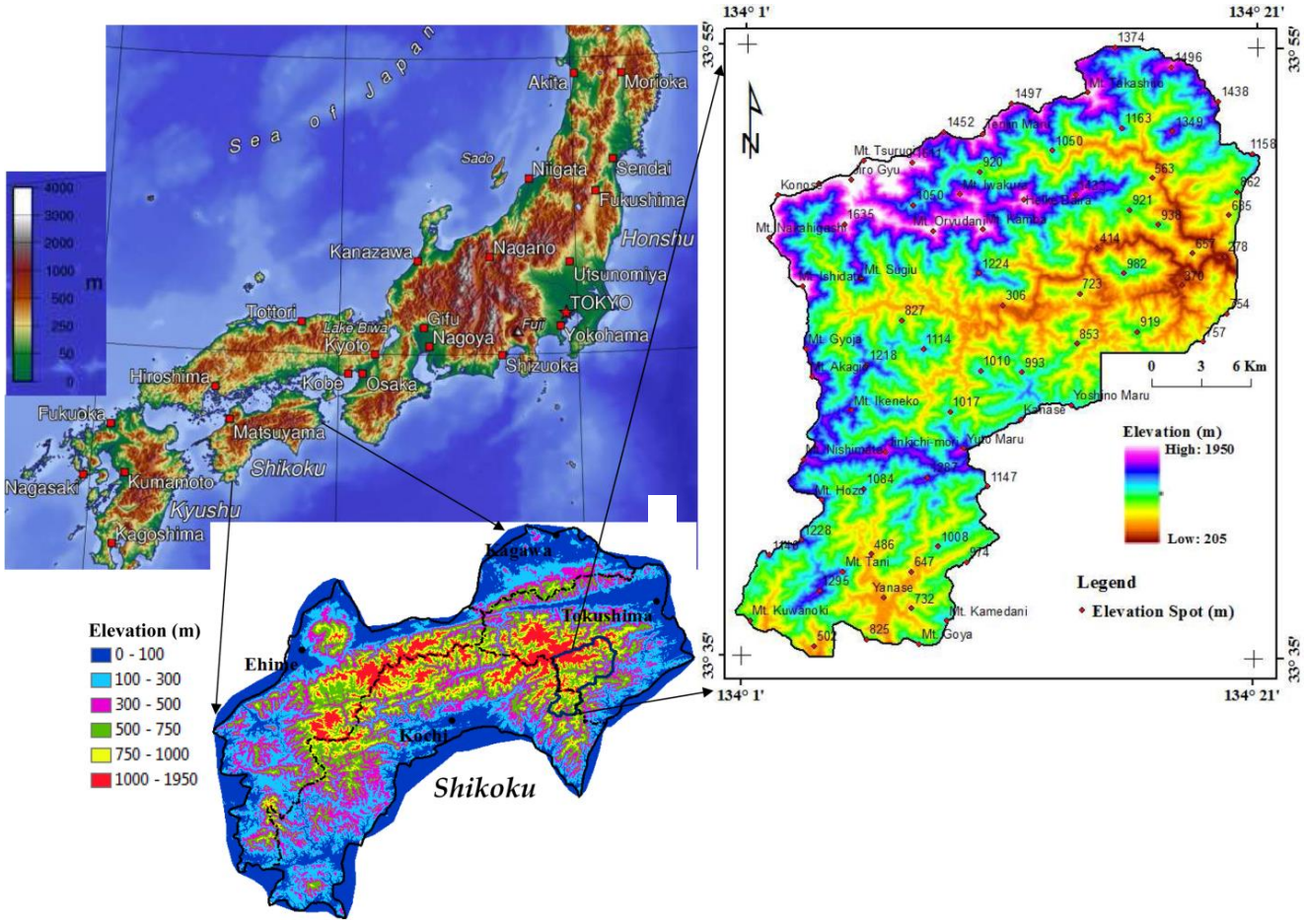

Fig. 1 Location map of the study area.

3. Literature Review

3.1 Effect of Rainfall on Landslide Occurrence in Shikoku

Landslides triggered by rainfall occur in most mountainous landscapes of the world (Dahal et al. 2008a). In Japan, precipitation occurs mostly during typhoon seasons on the Pacific Ocean side and in winter (heavy snow) on the Japan Sea side. Many types of landslides occur after heavy rainfall in tropical and temperate climatic zones. Shikoku Island has a humid climate with a mean annual precipitation of more than 2000 mm. Precipitation is largely brought by seasonal frontal systems and Typhoons that generate intense rainfall after which landslide disasters such as slope failures and debris flows frequently occur (Hong et al. 2005). Seasonal and torrential rainfall is the most important meteorological factor that can accelerate the movement of the sliding mass with a marked increase in landslide displacement (Hong et al. 2005; Wang et al. 2010).

The climatic conditions of Shikoku Island gave rise to seasonal and high intensity rainfall that caused landslide reactivation leading to deformation and collapseof buildings, roads and debris-slide control works in landslide prone areas. This active triggering factor affected the stability of crystalline schists in Shikoku Island therby promoting landslide movement (Hong et al. 2005). A huge number of landslides were also triggred in Tokushima Prefecture with

some catastrophic landslides in Kisawa village causing the loss of two lives and damage of roads from the typhon event that hit Shikoku from July 30 to August 2, 2004 with a daily precipitation of 1317 mm that surpassed the historical daily rainfall record of 1114 mm in Japan. During this time, precipitation also exceeded 1500mm for the storm event and landslides occurred within a narrow area in Kisawa Village and Kaminaka town (Wang et al. 2006; Wang et al. 2010).

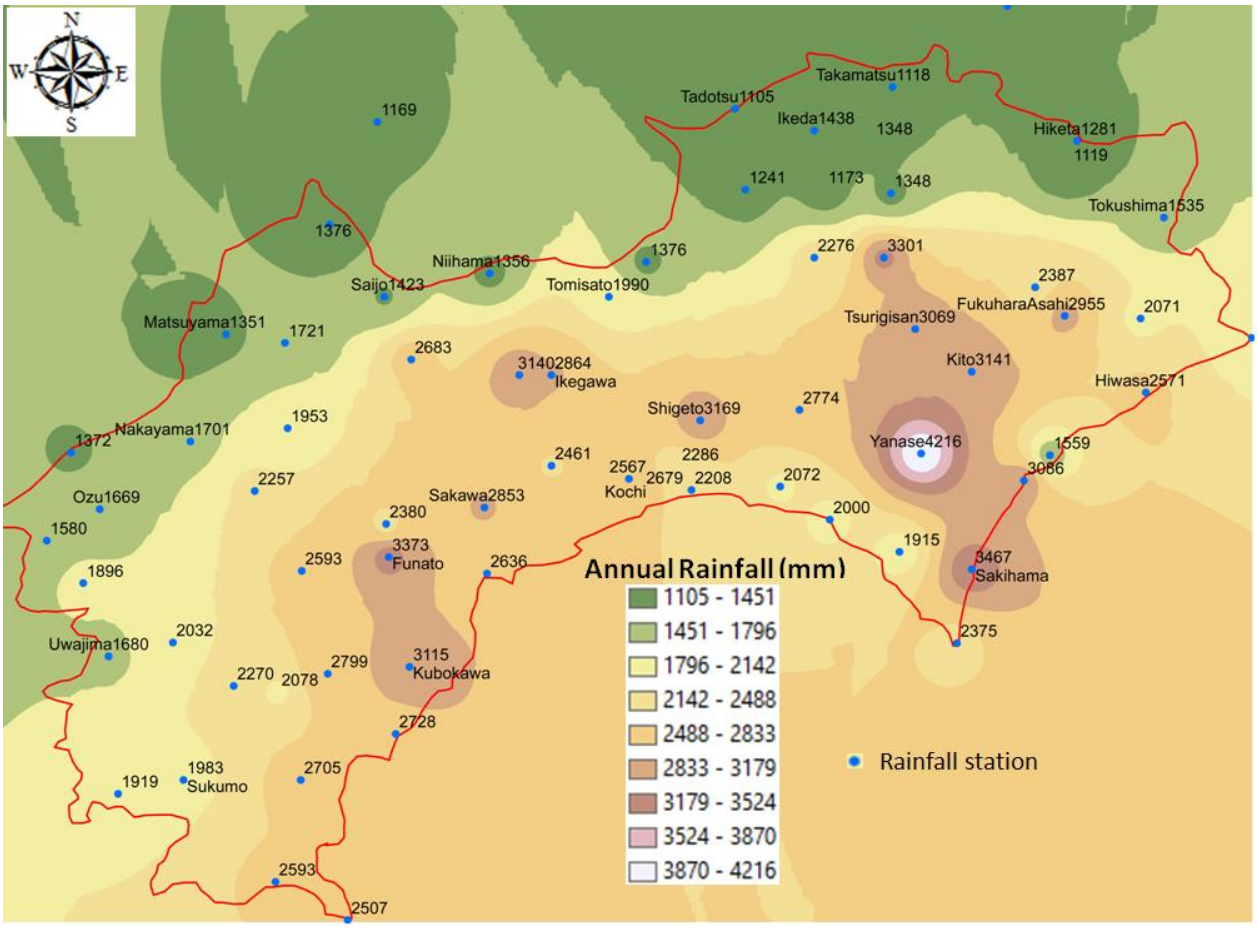

Fig. 2 Thirty years average annual rainfall of Shikoku Island.

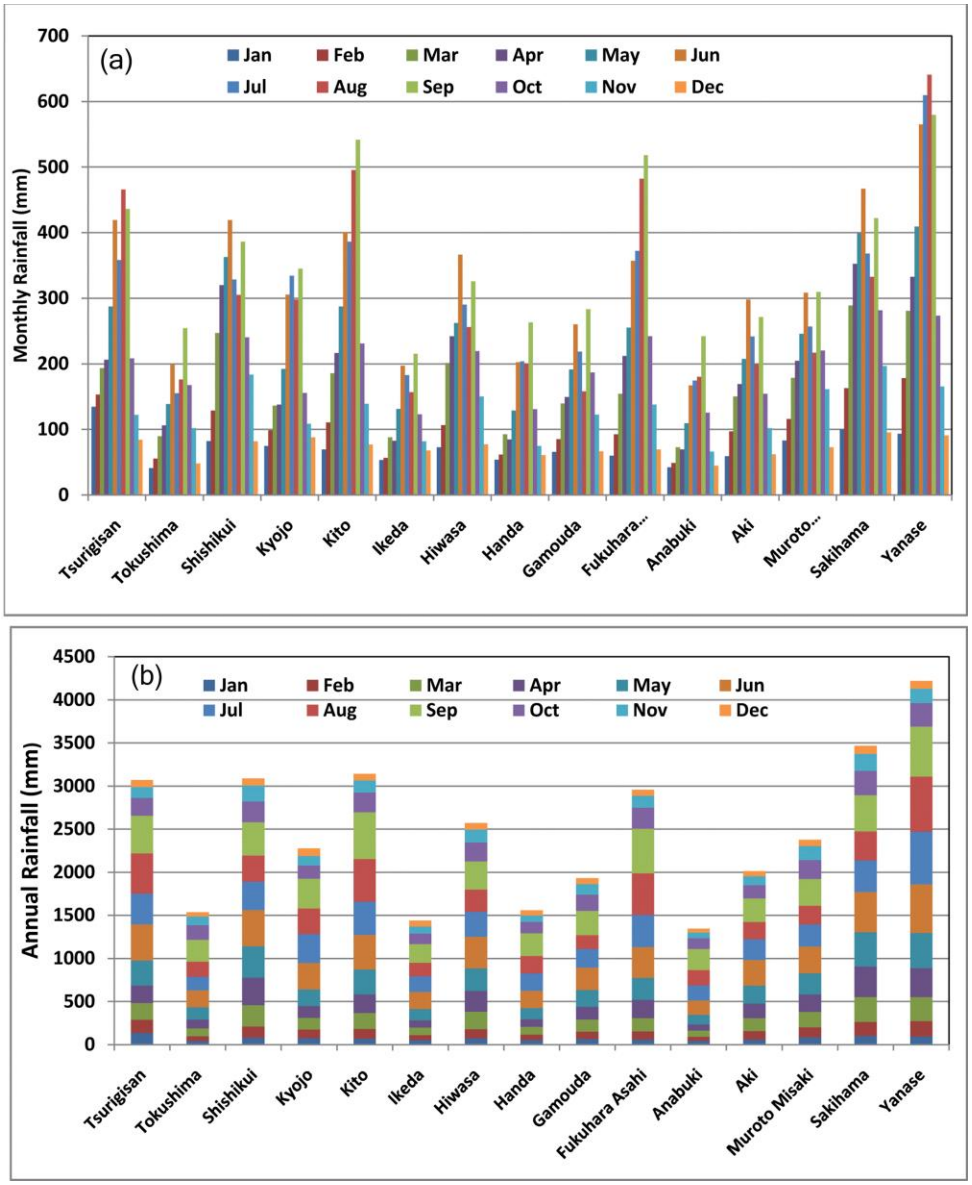

Fig. 3 Thirty year's average rainfall (1985 - 2014) showing (a) Monthly rainfall (b) Annual rainfall of the study area.

3.2 Effect of Geology on Landslide Ocurrence in Shikoku

From north to south, Shikoku Island can be roughly divided into three geological zones: Ryoke, Sambagawa-Chichibu and Shimanto belts. The three zones are bounded by two northerly dipping major faults, the Median Tectonic Line (MTL) and the Butsuzo Tectonic Line (BTL) from north to south respectively. The Ryoke Belt consists of late Cretaceous granitic rocks, late Cretaceous sedimentary rocks (Izumi Group) and Miocene volcanic rocks (Sanuki Group). Cretaceous granite is widely distributed in the north of Seto Inland Sea. Topographically MTL marks a distinct sharp boundary for Shikoku Range. This range, with a maximum altitude of nearly 2000 m, is occupied by the Sambagawa-Chichibu Belt. The Sambagawa Belt is composed of low-grade metamorphic rocks. The southern Chichibu Belt is mainly composed of Carboniferous to Jurassic sedimentary rocks and low grade metamorphic rocks. The

Shimanto Belt consists of Cretaceous and Palaeogene sedimentary rocks and this belt occupies the two southern peninsulas protruding into the Pacific Ocean. The middle Miocene granitic and partially gabbroic rocks are sporadically distributed along the axes of Muroto and Ashizuri peninsulas (Dahal et al. 2008a).

Four major tectonic lines cut through the central part of the island. These are the Median Tectonic Line, the Mikabu Tectonic Line, the Butsuzo Tectonic Line and Aki-Sukumo Tectonic Line which separate the geology of the Shikoku Island into five major geological belts including the Sanbagawa belt, the Chichibu belt, the Shimanto-northbelt, the Shimanto-south belt and the Ryoke belt (Hong et al. 2005). Many landslides have been found along the southern side of the Median Tectonic Line. The geology of these landslide sites are mainly comprised of crystalline schists including politic schist, green schist, psammitic schist and siliceous schist (Hong et al. 2005).The areas where the landslides occurred are characterized by deep river valleys with steep slopes and many of the mountain slopes have steep chutes. Most of the settlements are located on gentle slopes formed by past landslides or on narrow streamside terraces. According to the geological map of Tokushima Prefecture, the area is mainly underlain by Paleozoic greenstone, Paleozoic and Mesozoic pelite and greywacke and serpentinite of the Mesozoic Kurosegawa terrane as well as limestone and chert (Wang et al. 2006). However, the basal sliding surface occurred mainly within weathered serpentinite (Wang et al. 2010).

The geology of Niihama on the other hand consists of green schist of the Sambagawa Belt in the south and sandstone and shale of the Izumi Group in the north. This geological belt is primarily made of sedimentary deposits of sandstone with frequent intercalation of shale (Dahal et al. 2008a).

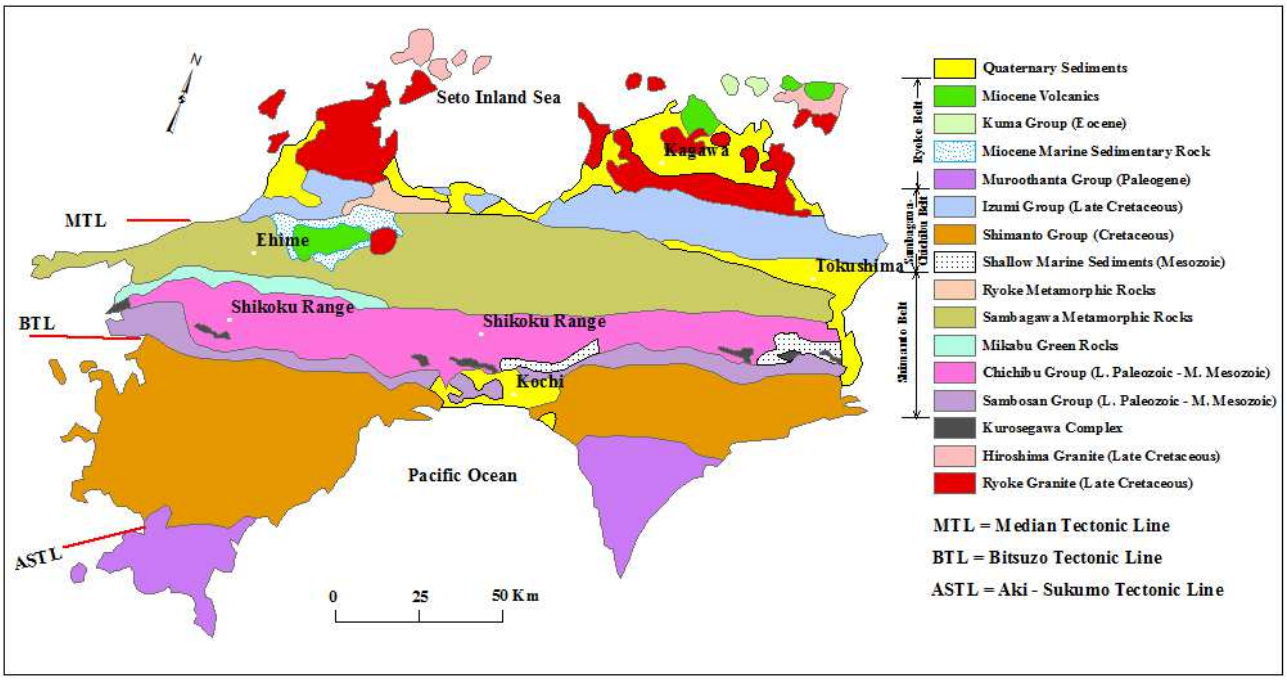

Figure **4** Simplified geological map of Shikoku Island (modified after Dahal et al. 2006)

3.3 Landslide Sites and Mechanisms in Shikoku

Many landslides were triggered by heavy rainfall (storm); the most catastrophic among them were five giant landslides occurring in Kisawa villages of the Nakagawa District in Tokushima Prefecture, namely the Oyochi, Kashu, Azue, Kamagatani and Shiraishi landslides.These landslides destroyed houses, forests and farms and damaged roads. Two people were buried inside Oyochi landslide and their bodies were never recovered. A catastrophic failure that occurred in the upper part of the Furon Valley in Shiraishi district destroyed more than 10 houses. Its basal sliding surface occurred within a weathered serpentinite. After the typhoon, the landslide was actively moving endangering the downstream residents (Wang et al. 2010).

Hong et al. (2005) investigated four crystalline schist landslides known as Zentoku, Kashio, Nishi-Igawa and Tsubayama in northwest of Tokushima prefecture that have been monitored for many years due to their continuous threat to the lives and properties of the local community. These landslides are classified as translational movements in weathered rock with deep-seated, continuous and creeping movement. The Zentoku landslide, located at Nishiiya village in Tokushima prefecture, is a large-scale crystalline schist landslide. The sliding mass is mainly composed of weathered and fractured green schist and pelitic schist. The Kashio landslide is located at Higashiiya village in Tokushima prefecture. Since 1988, the Japan Forestry Agency has systematically surveyed this large-scale landslide with the purpose of stabilizing the slope. The sliding mass is pellitic schist and the slip layer was found at varying depth levels of 20 **-** 50 m. The Nishi-igawa landslide is situated at the northern edge of the Sanbagawa belt and is very close to the Median Tectonic Line. It is smaller than the previous two slides and occupies about 6 ha in area with a length of 300 m and width of 200 m.The sliding mass is comprised of pelitic schist and siliceous schist. The landslide movement became apparent in 1973 due to an excavation at the toe of the slope. The Tsubayama landslide, which is located near the town of Ikegawa in Kochi prefecture, was identified by the Ministry of Construction of Japan in 1980 and became active in 1999 (Hong et al. 2005). The landslide is 500 m in length and 340 m in width and the sliding mass mainly consists of psammitic and pelitic schist.

In Kisawa village and its environs in Tokushima prefecture, five landslides were triggered on August 1, 2004 following a heavy typhoon rainfall. These include Oyochi, Kashu, Azue, Kamagatani and Shirashi landslides (Wang et al. 2006). The Oyochi and Kashu landslides occurred on the same side of a ridge. In Oyochi area, the bedrock is mainly composed of greenstone and serpentinite with visible cracks. Kashu landslide occurred on the same slope near the Oyochi landslide and occurred almost at the same time with the Oyochi event. Azue landslide is located on the left side of Sakashu-Kito River, in front of the Kashu landslide. A remarkable scar indicating an ancient landslide was also visible at this site (Wang et al. 2006). The displaced material slid down the slope, crossed Sakashu-Kito River and rose up the opposite mountain slope to a height of about 30 m (immediately below the Fudono area), destroying and carrying away the Fudono bridge, which was built on the national road. The main failure of Azue landslide occurred at approximately 23:00 hr on August 1, a little later than the Oyochi and Kashu landslides. Afterwards, loud crushing noises continued for several hours, probably due to retrogressive failures (Wang et al. 2006). The unstable landslide mass was estimated to be in the order of 10^6 m^3. This landslide mass was being deformed and the displacements measured by the installed extensometers showed that its movement was very sensitive to rainfall. Kamagatani landslide is located on the true right

slope of the valleys of Kamagatani River and the upper tributary of Sakashu-Kito River (Wang et al. 2006). The source area consists of mudstone, which is overlain by sandstone and ancient colluvial deposits. Shiraishi area was designated as the landslide prevention area on 1962, basing on the Japanese Landslide Preventive means and the mountain stream was also designated as the debris-flow-risk stream (Wang et al. 2006).

Dahal et al. (2008a) provided a detail account of the landslide disasters associated with the 2004 typhoon events in Tokushima, Kagawa, Ehime and Kochi prefectures of the Shikoku Island. Accordingly, from late July to early August, typhoon 10 brought heavy rainfall of more than 2000 mm to the southern part of Shikoku. This rainfall created four huge landslides around the Kisawa village of the Nakagawa district in Tokushima prefecture, occurring mainly at Oyochi, Kashu, Azue and Shiraishi area (Dahal et al. 2008a).

In 2004, typhoons 4, 6, 10, 11, 15, 18, and 23 hit Kochi Prefecture. Rainfall caused by typhoon 15 (Megi) induced many landslides in the Yoshino River basin of Shikoku on 17th - 18th August. Reihoku District in Kochi Prefecture was greatly affected by typhoon 15. Okawa and Uwezugawa villages were severely damaged. Many landslides occurred along the roadside slopes too. As a result, Okawa was isolated from the other parts of the prefecture (Dahal et al. 2008a).

The Okawa area mainly consists of crystalline green schist of the Sambagawa Belt, which includes pelitic schist, psammitic schist, and siliceous schist. There are thin to thick deposits of quaternary colluvium on the mountain slope of Yoshino River Valley. The crystalline schist is usually well known for landslide hazard and the sliding mass mainly consists of weathered and jointed schist (Hong et al. 2005; Dahal et al. 2008a).

Because of the thick forest in unpopulated hills, many landslides were only recognized long after the event. Researchers were still observing unreported small to medium-sized landslides triggered by the typhoon rainfall of 2004 in the forest of central Shikoku Island. Nevertheless, the International Sabo Association of Japan stated that nearly 600 types of slope failures have occurred in Shikoku during the 2004 typhoon events (Dahal et al. 2008a). Field observations of more than 250 slides in all prefectures indicated that both sliding and flowing are critical to the failure process. Various research studies established the nomenclature and classification of landslides in Shikoku, coming up with different terms used for such failures like debris flows, debris avalanche, soil slips, debris slides, flow-like landslides,slide-flows and so forth (Cruden and Varnes, 1996; Dahal et al. 2008a).

In a general sense, landslides in Shikoku Island after the 2004 typhoon events can be divided into translational slides, rotational slides, and a combination of both on the basis of the shape of the failure surface. The translational slides were found to be the most predominant failure mode of debris slide (Dahal et al. 2008a). Many of the landslides (e.g., Moriyuki, Monnyu,Toyohama, Okawa, and Kisawa) where translational debris slides occurring first on steep zero- order valley or concave slope and debrismaterials were run down through first-order stream channel (Dahal et al. 2008a). The flow continued to erode its route and either piled up huge debris at the mouth of the stream or continued traveling through the second-order stream for a considerable distance on the sloping terrain (Dahal et al. 2008a). Shallow failures are usually triggered by comparatively short, intense storms, whereas most of the deep-seated landslides were affected by long term variation of annual rainfall and daily rainfall (Hong et al., 2005).

4. Data Layers

4.1 Landslide Inventory

Landslide inventory maps document the extent of landslide phenomena in a region, and show information that can be exploited to investigate the distribution, types, pattern, recurrence and statistics of slope failures, to determine landslide susceptibility, hazard, vulnerability and risk, and to study the evolution of landscapes dominated by mass-wasting processes (Guzzetti et al. 2012). Having a high quality landslide inventory data, which depends on the accuracy, type and certainty of the information shown in the maps, will have a positive effect on the quality of landslide susceptibility, hazard and risk assessments (Guzzetti et al. 2012).

The landslide inventory data in the study area has been digitized from Google Earth Images (Figure 5) which were then converted in to GIS compatible format using kml to layer conversion tool. Then these landslides were checked against the georeferenced topraphic maps for their proper locations.

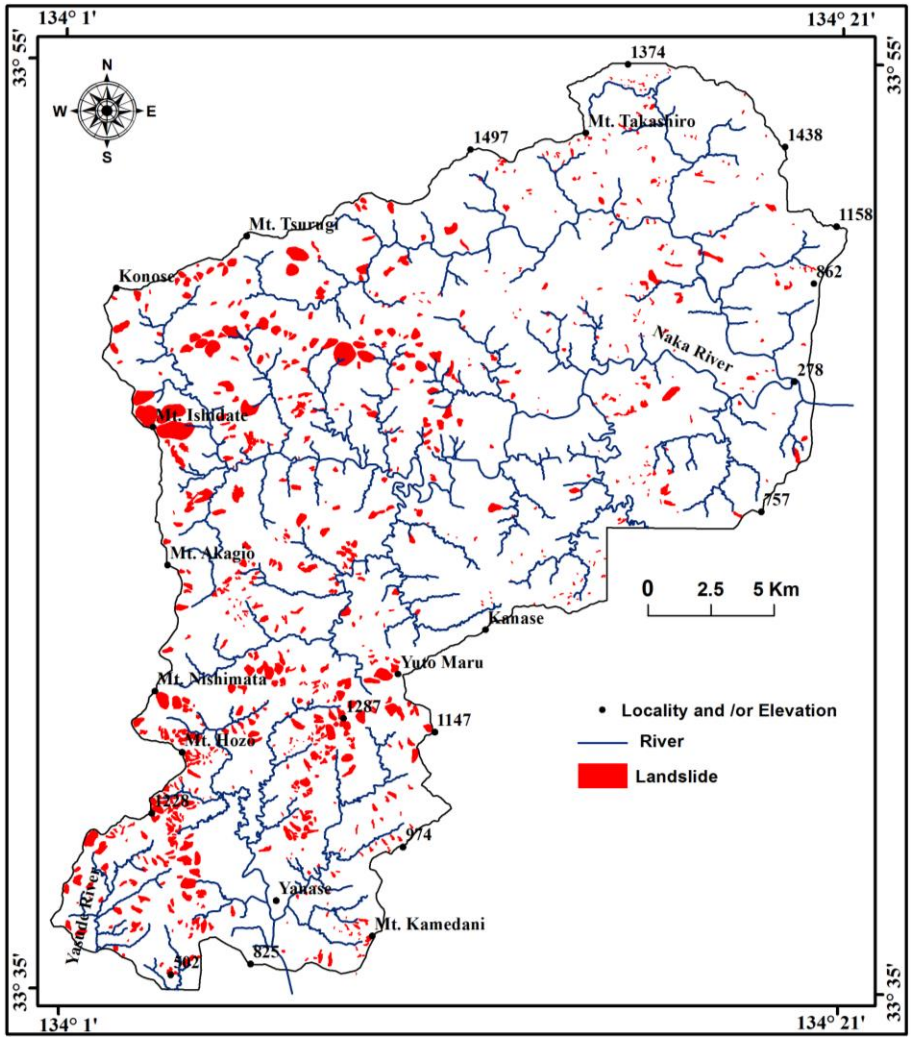

Figure 5 Landslide inventory map with river networks.

4.2 Landslide Factor Maps

The landslide factors considered in this study include slope, aspect, profile curvature, plan curvature, lithology, land use, distance from fault, distance from river and annual rainfall. Generally, the higher the slope, the higher will be the landslide density provided that the rock strength is low and the land use pattern falls in barren land to slightly vegetated bushes and shrubs. Slope orientation (aspect) affects the exposure to sunlight and to winds which in turn affects indirectly other factors that contribute to landslides such as precipitation, soil moisture, vegetation cover and soil thickness (Clerici et al., 2006). Curvature is the rate of change of slope gradient or aspect in a particular direction (Wilson and Gallant, 2000). Curvature controls the hydrological conditions of the soil cover. Curvature is generally divided into plan and profile (Ohlmacher, 2007). Profile and plan curvatures in particular affect the susceptibility to landslides. Profile curvature affects the driving and resisting stresses within a landslide in the direction of motion while plan curvature controls the convergence or divergence of landslide material and water in the direction of landslide motion (Carson and Kirkby, 1972). Curvature can be positive or convex (indicating peaks), negative or concave (indicating valleys) or zero (indicating flat surface or a saddle) (Pradhan, 2010; Alkhasawneh et al. 2013).
The main lithologic units (formations) in the study area include felsic plutonic rocks, ultramafic rocks, schist, marine sedimentary rocks, sandstones, muddy turbidite, mélange matrix, limestone, chert and basalt (www.gsj.jp/Map/EN/dgm.htm).

The land use classes of the study area, which have been digitized from Google Earth image include baren land, dense forest, reservoir, river and settlement.The land use pattern of the area has been changing due to cutting of trees for timber at selected sites.

The presences of faults also contribute significantly to landslide occurrence in the study area. As can be depicted from table 1, most of the landslides are concentrated in close proximity to faults. This shows that landslides are more frequent near to the close vicinity of faults.

The river dynamics can erode and incise areas along its channel and river banks. Hence landslides are more frequent close to rivers. In general, as the distance from river increases,the probability of landslide occurrence decreases. However, in the current study area, landslides are more frequent in intermidiate river distance classes between 400 – 1500m(Table 1). This may be due to the presence of dense vegetation and competent rocks along the river courses.

The rain gauge stations inside and in the vicinity of the study area shows a spatial variability in annual and monthly rainfall patterns (Figure 3 a & b) in which the maximum rainfall is recorded during the months of June, July, August and September.

The thirty years average annual rainfall records of rain gauge stations in Shikoku island from Japan Meteorology Agency(http://www.data.jma.go.jp/gmd/risk/obsdl/index.php)were used to interpolate the rainfall isohyets (Figures 2 and 6i).

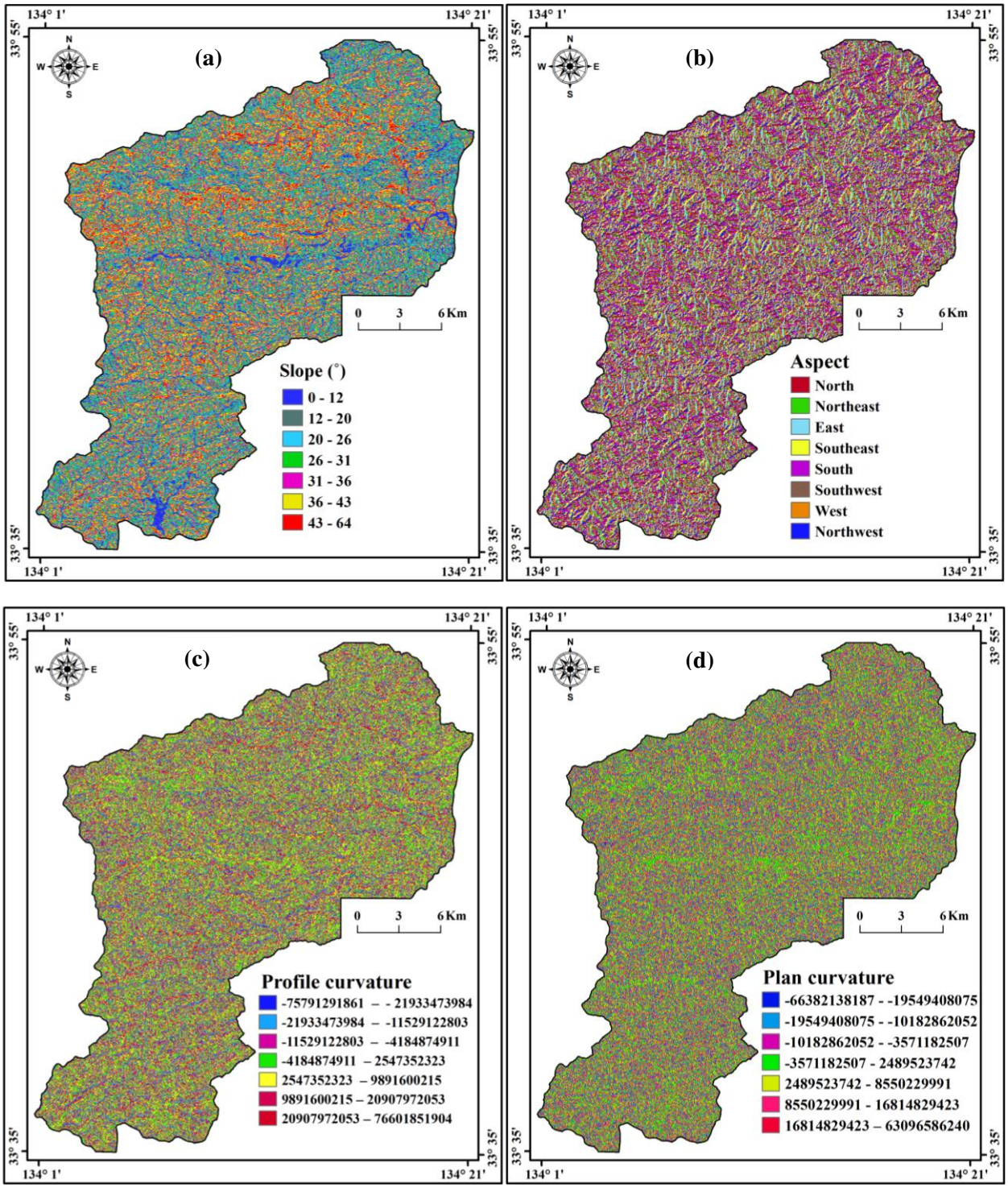

Figure 6 Landslide Factos (a) Slope (b) Aspect (c) Profile curvature (d) Plan curvature

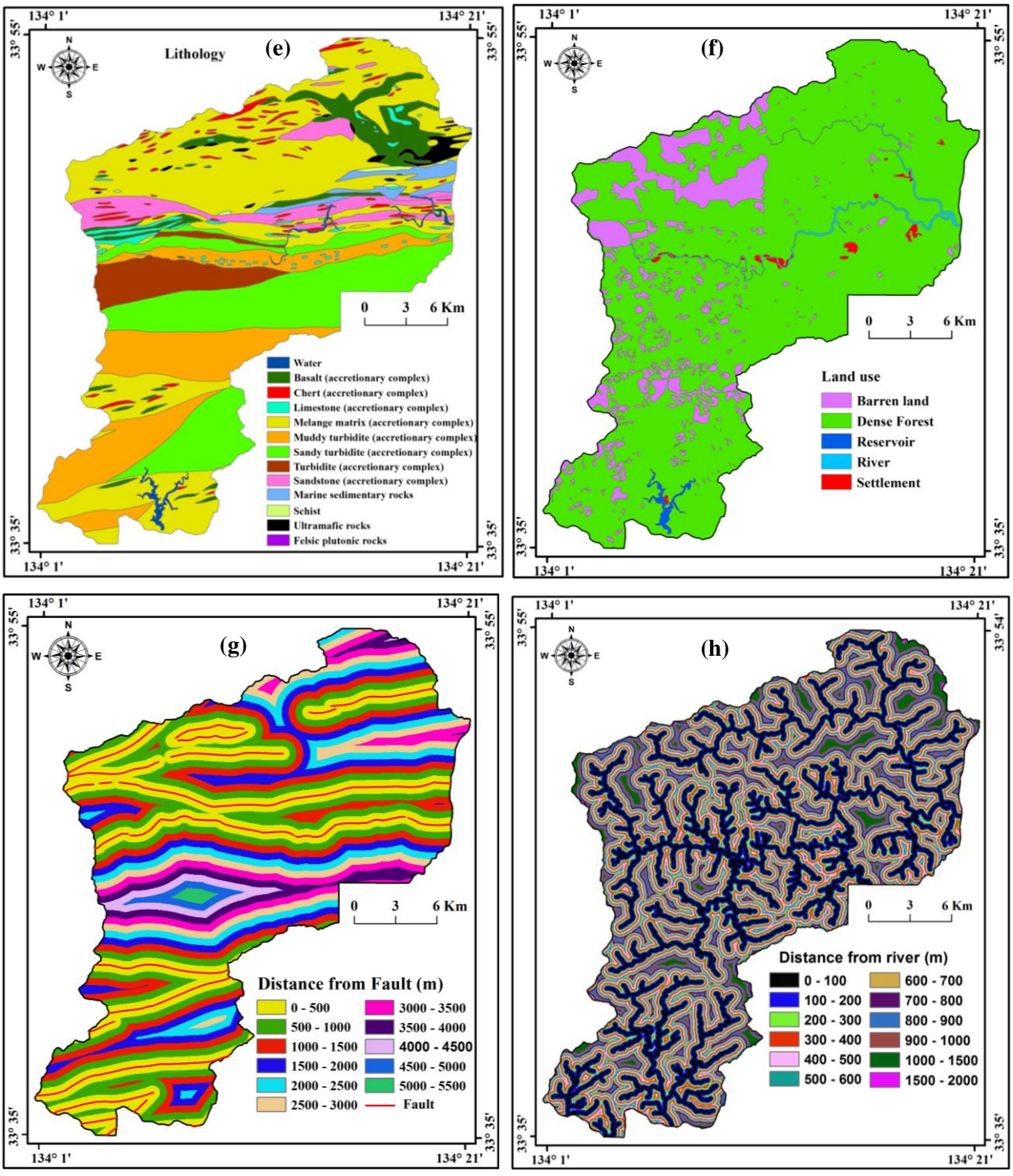

Figure 6 Landslide factors (e) Lithology (f) Land use (g) Distance from fault (h) Distance from river.

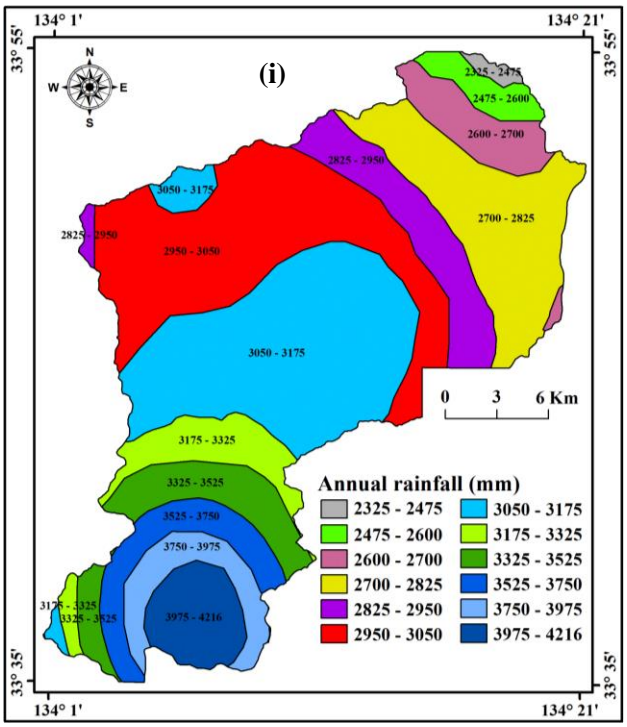

Figure 6 Landslide Factor (i) Annual rainfall.

5. Methods

5.1 Frequency Ratio

In order to get the best result for the frequency ratio method, two approaches have been applied(Figure 7 and table 1). The first one is using the frequency ratio value of Lee and Sambath (2006) and the second is to use the landslide density method of Ayalew and Yamagishi (2005). Among these two options, the latter was found to be appropriate as it resulted the highest Area Under the Curve (AUC) value of 0.867 compared to the former which is 0.865. Hence the landslide density method was applied as an input data for the other methods too.

$$FR = \frac{\frac{\#\ landslide\ pixels}{\sum_{i=1}^{n} \#\ landslide\ pixels}}{\frac{\#\ class\ pixels}{\sum_{i=1}^{n} \#\ class\ pixels}} \quad \text{.....(1)}$$

Where FR = the frequency ratio of each factor class, n= number of classes in a certain factor,# landslide pixels = number of landslide pixels in a certain factor class, $\sum_{i=1}^{n} \#$ landslide pixels = sum of all landslide pixels in the entire area, # class pixels = number of pixels in a certain class, $\sum_{i=1}^{n} \#$ class pixels = sum of all pixels in the entire area (Regmi et al., 2014).

The landslide density approach in the frequency ratio method can be calculated in the following manner.

$$\%\ \text{landslide pixels} = \frac{\#\ landslide\ pixels}{\sum_{i=1}^{n} \#\ landslide\ pixels} \quad \text{.....(2)}$$

$$\%\ \text{class pixels} = \frac{\#\ Class\ pixels}{\sum_{i=1}^{n} \#\ Class\ pixels} \quad \text{.....(3)}$$

$$\text{Density} = \frac{\#\ landslide\ pixels}{\#\ class\ pixels} \quad \text{.....(4)}$$

$$\% \text{ density} = \frac{\% \text{ landslide pixels}}{\% \text{ class pixels}} = \frac{\frac{\text{\# landslide pixels}}{\text{\# class pixels}}}{\sum_{i=1}^{n} \frac{\text{\# landslide pixels}}{\text{\# class pixels}}} * 100 \quad (5)$$

where n is the number of classes in a certain landslide factor.

$$\mathbf{LSI = Fr_1 + Fr_2 + Fr_3 + \ldots + Fr_n} \quad (6)$$

Where Fr_1, Fr_2, Fr_3… Fr_n are the frequency ratio or landslide density raster maps of of each landslide factor, LSI represents the landslide susceptibility index and n is the number of factors. If the LSI value is higher, it means a higher susceptibility to landslide but if LSI is lower, it means a lower susceptibility to landslides (Lee and Sambath, 2006; Lee et al., 2007).

5.2 Logistic Regression

Logistic regression is the most commonly used multivariate method as (1) it can be used to predict a result measured by a binary variable such as the presence or absence of landslides based on a set of one or more independent variables; (2) it does not require the variables to be normally distributed; (3) the independent variables can be non-linear, continuous, categorical or a combination of both continuous and categorical (Menard 1995; Schicker and Moon 2012; Meten et al. 2015b). It helps to form a multivariate regression analysis between a dependent variable and several independent variables (Lee 2005b; Shahabi et al. 2014). It is useful to predict the presence or absence of a characteristic outcome based on values of a set of predictor variables (Lee and Sambath 2006; Lee et al. 2007; Yilmaz 2009; Yalcin et al. 2011). The purpose of logistic regression is finding the best fit model to describe the relationship between a dependent variable and a set of independent variables (Ayalew and Yamagishi 2005). The dependent variable is coded as "1" and "0" representing the presence and absence of a landslide respectively (Atkinson and Massari 1998). The dependent variable is the landslide area. Then these areas are rasterized and converted into a point format in GIS. These pointsare in turn used to extract the values of individual frequency ratio density maps for each of the nine landslidefactors. These points were extracted in dBf format and can be accessed inSPSS statistical software. Then, they were saved in SPSS compatible format. The next step is to merge the landslide and non-landslide extracted points of the nine landslide factors separately (Meten et al. 2015b). Using logisticregression the spatial relationship betweenlandslides and landslide factors was established to determine coefficients of each independent variable (Akgün and Bulut 2007). After this calculation, the coefficients of the landslide factors were obtained as shown in Table 2. Quantitatively, the relationship between landslide occurrence and its dependency on several variables can be expressed in its simplest form in Eq. 7 (Lee and Sambath 2006; Akgün and Bulut 2007; Schicker and Moon 2012) as follows.

$$\boldsymbol{P = \frac{1}{1 + e^{-z}}} \quad (7)$$

Where *P* is the probability of landslide occurrence and *Z* is the linear combination.

Logistic regression involves fitting an equation of the following form to the data (Eq. 8):

$$\boldsymbol{Z = b_0 + b_1X_1 + b_2X_2 + b\ \ _3X_3 + \cdots b_nX_n} \quad (8)$$

Where b_0 is the intercept of the model, the b_i (i = 1, 2, 3 ....n) is the slope coefficients of the logisticregression model x_i (i = 1, 2, 3 ....n) are independent variables. The coefficients of landslide factors with positive values show a positive

correlation towards landslide occurrence while those with negative coefficients show a negative correlation (Yalcin et al. 2011).

In this study, a landslide susceptibility map with high prediction accuracy was selected. The prediction accuracy of the model was determined from area under the curve (AUC) values of the receiver operating characteristic (ROC) curves. For validation, the landslide inventory map was overlaid over the landslide susceptibility map and analyzed how much percentage of landslides fall in each susceptibility class. If majority of the landslides fall in the very high and high susceptibility classes, then the landslide susceptibility map is acceptable but if this is not the case, checking the quality of the data that were used in the analysis is needed (Figure 7).

5.3 Weights of Evidence

The weights of evidence modelling uses the Bayesian probability approach and was originally designed for mineral potential assessment (Bonham-Carter 1988; Bonham-Carter 1994). This method was also being applied in landslide susceptibility mapping in the past three decades (Van Westen et al. 2003; Lee et al. 2004; Dahal et al. 2008b; Regmi eta al. 2010b). If F represents the presence and $\overline{\mathbf{F}}$ represents absence of a potential landslide factor and if L represents the presence and $\overline{\mathbf{L}}$ represents absence of landslide, then WoE model calculates the positive and negative weights of the respective factor classes based on the probability ratios (Bonham- Carter 2002) in the following manner**.**

$$W^{+} = log_{e}\left(\frac{P\{F|L\}}{P\{F|\overline{L}\}}\right) \tag{9}$$

$$W^{-} = log_{e}\left(\frac{P\{\overline{F}|L\}}{P\{\overline{F}|\overline{L}\}}\right) \tag{10}$$

A positive weight (W_i^+) indicates presence of a causative factor in the landslide and the magnitude of this weight is an indication of the positive correlation between presence of the causative factor and landslides. A negative weight (W_i^-) indicates an absence of the causative factor and the magnitude indicates negative correlation. The difference between the two weights is known as the weight of contrast, C where ($C = W_i^+ - W_i^-$) and the magnitude of contrast reflects the overall spatial association between the causative factor and landslides (Dahal et al. 2008b; Regmi et al. 2010b). If the weight contrast is positive, the factor is favorable to cause landslides and if it is negative, it will be unfavorable for the occurrence of landslides. If it is close to zero, this indicates that the factor shows minor relation to landslides. In order to calculate the weights of each landslide factor classes for landslide susceptibility mapping, Eqs. (9) and (10) were expressed in terms of the numbers of cells (pixels) as follows.

$$W^{+} = log_{e}\left(\frac{\frac{npix1}{npix1+npix2}}{\frac{npix3}{npix3+npix4}}\right) = log_{e}\left(\frac{\frac{\text{landslides inside the class}}{\text{landslide inside the class + landslide outside the class}}}{\frac{\text{non-landslide inside the class}}{\text{non-landslides inside and outside the class}}}\right) \tag{11}$$

$$W^{-} = log_{e}\left(\frac{\frac{npix2}{npix1+npix2}}{\frac{npix4}{npix3+npix4}}\right) = log_{e}\left(\frac{\frac{\text{landslides outside the class}}{\text{landslide inside the class + landslide outside the class}}}{\frac{\text{non-landslide outside the class}}{\text{non-landslides inside and outside the class}}}\right) \tag{12}$$

Where nslclass is the number of landslide pixels in a certain factor class, nslide is the number of landslide pixels in the entire area, nclass is the number of pixels in a certain factor class, nmap is the number of pixels in the entire area, npix1 is the number of landslide pixels present on a given factor class, npix2 is the number of landslides pixels not present in a given factor class, npix3 is the number of pixels in a given factor class in which no landslide pixels are present and npix4 is the number of pixels in which neither landslide nor the given factor is present (Van Westen, 2002, Sharma and Kumar, 2008, Dahal et al., 2008b; Regmi et al., 2010b).

The steps in the initial stage of WoE modeling include preparing the landslide factors, landslide inventory maps and converting them into a raster format with the same geographic projection and same pixel size of 30 m followed by calculating the number of landslide pixels in each factor's class (npix1), the number of total landslide pixels in the whole study area (nslide), the number of pixels in each factor's class (nclass), the difference between the total number of landslide pixels from landslide pixels in each factor's class (npix2), the difference between the number of pixels in the factor's class from the landslide pixels in that class (npix3) and the number of non-landslide pixels in the entire area (npix4) using Arc GIS 10 (Table 4). Then positive and negative-weights were calculated, the final weights of contrast values were determined from the difference of these weights for each factor class in Microsoft Excel and these contrast decimal values were changed in to integers by multiplying them with an appropriate multiples of 10 since assigning decimal values was not possible in Arc GIS 10. In order to transform the negative values into values with greater or equal to zero, the least negative number is subtracted from each class value in the factor using Microsoft excel. The next steps were assigning the newly transformed positive values to the respective factor classes using the reclassify option of the spatial analyst tool in ArcGIS, converting the resulting raster map of each factor into a float format using raster to float conversion, converting the resulting float format of each factor into raster using float to raster conversion tool, adding the transformed value of the smallest negative integer in each factor with the output raster map, divide the resulting map with an appropriate multiple of 10 that was used for changing the decimal into integers in Arc GIS. Then, a continuous raster map of a certain factor representing the weights of evidence contrast values was obtained.

Repeating the above procedures enables to prepare all the weights of evidence contrast values with a continuous raster map of the real weights of originally calculated values such as decimals of positive, negative or zero values. Before adding the raster contrast values of all the landslide factors, statistical independence test of landslide factors among each other and with landslide inventory map was carried out using logistic regression method. Then, the raster contrast values of all landslide factors that were conditionally independent were added to get the landslide susceptibility index map which was then reclassified into five susceptibility classes based on natural breaks method. Finally the landslide susceptibility index map was extracted using landslide points which have been used in the analysis in order to get ROC (receiving operational characteristic) curve, AUC (area under the curve) and the prediction accuracy of the landslide susceptibility map. The entire procedure in implementation of this model can be seen from figure 7.

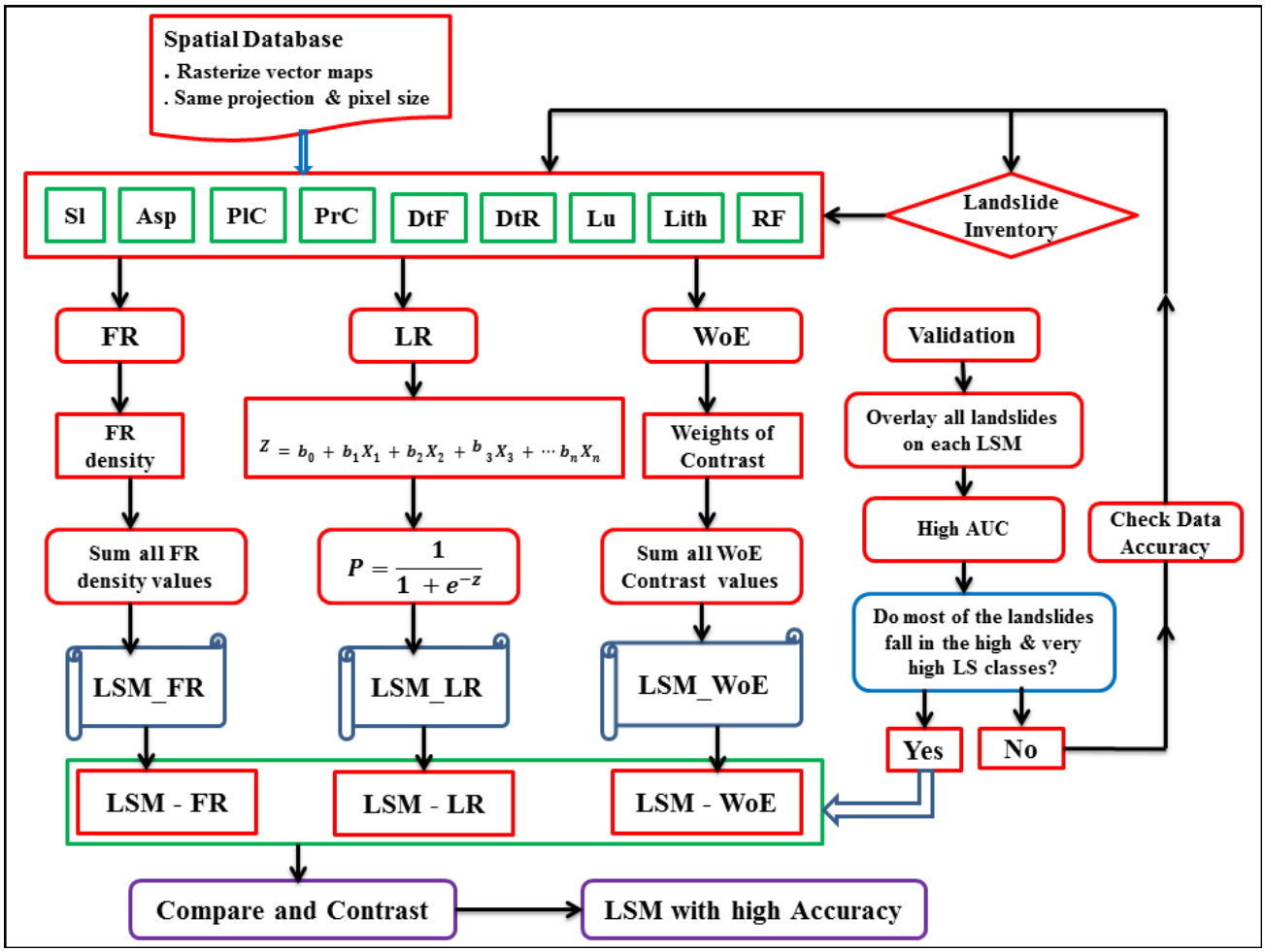

Figure 7 Flow chart of the work(Sl = slope, Asp = aspect, Prc = profile curvature, Plc = plan curvature, Lith = lithology, DtF = distance to fault, DtR = distance to river, Lu = landuse, AR = Annual Rainfall, FR =Frequency Ratio,LR = Logistic Regression, WoE =Weights of Evidene and LS = Landslide Susceptibility, LSM =Landslide Susceptibility Map and AUC = Area Under the curve).

6. Result and Discussion

6.1 Frequency Ratio

From Table 1, it can be seen that the frequency ratio (FR) values >1 and the frequency ratio density values ≥ 0.0458 that have a significant contribution to landsliding include aspect(S, SW, W & NW); distance from fault (0-500m, 500 – 1000m, 1000 – 1500m, 4500 – 5000m, 5000 – 5500m); land use (barren land); lithology(mélange matrix, muddy turbidite, basalt, limestone & felsic plutonic rocks); slope (31° - 36°, 36° - 43° & 43° - 64°), annual rainfall (2950 -3050 mm, 3175 – 3325mm, 3325 – 3525mm,3525 – 3750mm, 3750 – 3975mm); plane curvature (the first three classes with negative values) and profile curvature (the first two negative classes and the last two positive classes).

Table 1 Frequency Ratio and landslide density values.

Factor	Class	# class pixels	% class pixels	# landslide pixels	% landslide pixels	FR	density	% density
Aspect	N	97024	14.56	4231	13.92	0.96	0.0436	12
	NE	74356	11.16	3223	10.61	0.95	0.0433	12
	E	81209	12.19	2993	9.85	0.81	0.0369	10
	SE	80853	12.13	3705	12.19	1.00	0.0458	13
	S	113022	16.96	5545	18.25	1.08	0.0491	13
	SW	58326	8.75	2694	8.86	1.01	0.0462	13
	W	80839	12.13	4064	13.37	1.10	0.0503	14
	NW	80731	12.12	3936	12.95	1.07	0.0488	13
Distance	0 - 500	162042	24.32	9629	31.68	1.30	0.0594	12
from fault (m)	500 - 1000	136865	20.54	7719	25.40	1.24	0.0564	12
	1000 - 1500	104054	15.62	5032	16.56	1.06	0.0484	10
	1500 - 2000	76013	11.41	3120	10.27	0.90	0.0410	8
	2000 - 2500	54841	8.23	1395	4.59	0.56	0.0254	5
	2500 - 3000	46704	7.01	1127	3.71	0.53	0.0241	5
	3000 - 3500	37865	5.68	668	2.20	0.39	0.0176	4
	3500 - 4000	25115	3.77	610	2.01	0.53	0.0243	5
	4000 - 4500	13202	1.98	454	1.49	0.75	0.0344	7
	4500 - 5000	7127	1.07	388	1.28	1.19	0.0544	11
	5000 - 5500	2532	0.38	249	0.82	2.16	0.0983	20
Distance	0 - 100	115661	17.36	1755	5.77	0.33	0.0152	2
from River (m)	100 - 200	102258	15.35	2934	9.65	0.63	0.0287	5
	200 - 300	92563	13.89	3432	11.29	0.81	0.0371	6
	300 - 400	83098	12.47	3683	12.12	0.97	0.0443	7
	400 - 500	72855	10.93	3869	12.73	1.16	0.0531	8
	500 - 600	61099	9.17	4128	13.58	1.48	0.0676	11
	600 - 700	48973	7.35	3764	12.39	1.69	0.0769	12
	700 - 800	36263	5.44	2721	8.95	1.65	0.0750	12
	800 - 900	23787	3.57	1862	6.13	1.72	0.0783	12
	900 - 1000	14040	2.11	1191	3.92	1.86	0.0848	13
	1000 - 1500	15539	2.33	1052	3.46	1.48	0.0677	11
	1500 - 2000	224	0.03	0	0	0.00	0.0000	0
Land use	Dense Forest	575208	86.32	9648	31.75	0.37	0.0168	6
	Barren land	78500	11.78	20743	68.25	5.79	0.2642	94
	Reservoir	3187	0.48	0	0.00	0.00	0.0000	0
	Settlement	3637	0.55	0	0.00	0.00	0.0000	0
	River	5828	0.87	0	0.00	0.00	0.0000	0
Lithology	Melange matrix	250566	37.60	12614	41.51	1.10	0.0503	4
	Muddy turbidite	112377	16.86	6049	19.90	1.18	0.0538	4
	Water	5172	0.78	9	0.03	0.04	0.0017	0
	Sandy turbidite	135882	20.39	4649	15.30	0.75	0.0342	3
	Basalt	40895	6.14	1989	6.54	1.07	0.0486	4
	Chert	14776	2.22	422	1.39	0.63	0.0286	2
	Turbidite	35583	5.34	1336	4.40	0.82	0.0375	3
	Limestone	9882	1.48	1358	4.47	3.01	0.1374	11
	Sandstone	39379	5.91	1630	5.36	0.91	0.0414	3
	Schist	2041	0.31	76	0.25	0.82	0.0372	3
	Ultramafic rocks	7714	1.16	118	0.39	0.34	0.0153	1
	Marine sedimentary rocks	11997	1.80	72	0.24	0.13	0.0060	0
	Felsic plutonic rocks	96	0.01	69	0.23	15.76	0.7188	59

Note: # = number of, density = (# landslide pixels /# class pixels), Frequency Ratio (FR) = (% landslide pixels / % class pixels)

Table 1 (... continued) Frequency Ratio and landslide density values.

Factor	Class	# class pixels	% class pixels	# landslide pixels	% landslide pixels	FR	density	% density
Plan Curvature	-66382138137 - - 19549408075	15736	2.36	1219	4.01	1.70	0.0775	22
	-19549408075 - - 10182862052	68475	10.28	4335	14.26	1.39	0.0633	18
	-10182862052 - - 3571182507	136644	20.51	7102	23.37	1.14	0.0520	15
	-3571182507 - 2489523742	184216	27.65	7916	26.05	0.94	0.0430	12
	2489523742 - 8550229991	147853	22.19	5709	18.79	0.85	0.0386	11
	8550229991 - 16814829423	86120	12.92	3132	10.31	0.80	0.0364	10
	16814829423 - 63096586240	27316	4.10	978	3.22	0.79	0.0358	10
Profile Curvature	-75791291861 - - 21933473984	17691	2.65	916	3.01	1.14	0.0518	15
	-21933473984 - - 11529122803	68432	10.27	3209	10.56	1.03	0.0469	14
	-11529122803 - - 4184874911	132659	19.91	5884	19.36	0.97	0.0444	13
	-4184874911 - 2547352323	180925	27.15	7843	25.81	0.95	0.0433	13
	2547352323 - 9891600215	156080	23.42	7038	23.16	0.99	0.0451	13
	9891600215 - 20907972053	88606	13.30	4265	14.03	1.06	0.0481	14
	20907972053 - 76601851904	21967	3.30	1236	4.07	1.23	0.0563	17
Annual Rainfall (mm)	2475 - 2600	14500	2.18	72	0.24	0.11	0.0050	1
	2950 - 3050	144279	21.65	10003	32.91	1.52	0.0693	14
	3325 - 3525	42939	6.44	4338	14.27	2.22	0.1010	20
	3750 - 3975	28558	4.29	1790	5.89	1.37	0.0627	13
	2325 - 2475	3497	0.52	4	0.01	0.03	0.0011	0
	2700 - 2825	89956	13.50	1108	3.65	0.27	0.0123	2
	2600 - 2700	29332	4.40	479	1.58	0.36	0.0163	3
	2825 - 2950	50051	7.51	954	3.14	0.42	0.0191	4
	3175 - 3325	35212	5.28	2372	7.80	1.48	0.0674	13
	3525 - 3750	33821	5.08	2888	9.50	1.87	0.0854	17
	3975 - 4216	31501	4.73	845	2.78	0.59	0.0268	5
	3050 - 3175	162714	24.42	5538	18.22	0.75	0.0340	7
Slope (˚)	0 -12	41717	6.26	570	1.88	0.30	0.0137	4
	12 - 20	87186	13.08	2427	7.99	0.61	0.0278	9
	20 - 26	115353	17.31	4584	15.08	0.87	0.0397	13
	26 - 31	124866	18.74	5631	18.53	0.99	0.0451	15
	31- 36	127043	19.07	6727	22.13	1.16	0.0530	17
	36 - 43	124735	18.72	7171	23.60	1.26	0.0575	19
	43 - 64	45460	6.82	3281	10.80	1.58	0.0722	23
Note: # = number of, density = (# landslide pixels /# class pixels), Frequency Ratio (FR) = (% landslide pixels / % class pixels),								

6.2 Logistic Regression

In order to analyze the effects of data sampling on the prediction accuracy of landslide susceptibility maps in logistic regression method, two cases with equal- and unequal proportions of non-landslide points were combined with all landslide points. This helps to determine the coefficients of each landslide factor and other statistical parameters like -2 log likelihood, Cox and Snell R square, Chi-square, Nagelkerke R square and statistical significance (Table 2). The prediction accuracy also showed almost similar values n this study. Among the two cases, the data sampling/combinationof equal landslide points and non-landslide points showed the highest prediction accuracy of 86.8% (Table 3)..

Table 2 Logistic regression coefficients from unequal and equal proportion of landslide and non-landslide pixels and their model statistics.

Parameters	Coefficients from combination of all landslide and non-landslide pixels.	Collinearity Test		Coefficients from combination of equal landslide and non landslide pixels	Collinearity Test	
		Tolerance	VIF		Tolerance	VIF
Aspect	8.901	0.98	1.02	6.955	0.962	1.04
Distance from Fault	3.654	0.72	1.39	6.381	0.945	1.06
Distance from River	8.863	0.96	1.04	10.825	0.99	1.01
Land use	3.166	0.68	1.47	3.242	0.85	1.18
Lithology	4.799	0.8	1.25	4.823	0.88	1.14
Rainfall	4.404	0.75	1.33	6.080	0.913	1.1
Slope	7.295	0.95	1.05	6.961	0.97	1.03
Plan curvature	0	0.55	1.82	6.194	0.92	1.09
Profile curvature	0	0.6	1.67	-1.947	0.62	1.61
Constant	-8.164			-6.021		
-2 Log likelihood	182582.9			55186.6		
Cox & Snell R Square	0.092			0.38		
Nagelkerke R Square	0.298			0.507		
Chi Square	15.54			16.42		
Significance	0.063			0.072		

Table 3 Number of landslide and non-landslide pixels used in each model, area under the curve (AUC) values and success rate (%).

Analysis method	# Landslide pixels	# Non-landslide pixels	Area Under the Curve (AUC)	Success rate (%)
FR_density	30391	635969	0.867	86.7
FR	30391	635969	0.865	86.5
LR(equal landslide and non-landslide pixels)	30391	30391	0.868	86.8
LR(all landslide and non-landslide pixels)	30391	635969	0.864	86.4
Weights-of-Evidence (WoE)	30391	635969	0.807	80.7

Selecting a sample for logistic regression model involves considerations of the sample size and the proportion of landslide and non-landslide pixels (Schicker and Moon 2012). If there are many parameters, it would produce a long regression equation that may even create numerical problems and also may result in the absence of strong correlations (multicollinearity) among independent variables. A regression was performed among the independent parameters, not classes of parameters (Ayalew and Yamagishi 2005). In a logistic regression model, three approaches can be followed for data sampling purposes (Zhu and Huang 2006). The first one is using data from all over the study area, which leads to unequal proportions of landslide and non-landslide pixels (Guzzetti *et al*. 1999; Ohlmacher and Davis 2003).

The second approach is using the entire landslide pixels and equal proportions of non-landslide pixels. This may decrease number of data to be used but it eliminates the associated bias in the data sampling process (Zhu and Huang 2006). Yesilnacar and Topal (2005) used the total number of landslide pixels and randomly selected cells from landslide free areas. The third approach is to divide landslide pixels into two parts, i.e. training and validation data (Zhu and Huang 2006). There are also two cases in this approach.The first one is the application of unequal pixels (Atkinson and Massari 1998) and the second one is to use equal proportion of landslide and non-landslide pixels (Dai and Lee 2002). In order to tackle the drawbacks attributed to the application of unequal proportion of landslide and non-landslide pixels, equal numbers of non-landslide pixels are randomly selected from landslide free area and combined with equal number of landslide pixels for the logistic regression model in this study. A forward stepwise logistic regression method was applied in order to establish a relationship between the landslide and landslide factors. In order to get the best result from logistic regression analysis, multicollinearity and Hosmer-Lemeshow tests were considered (Zhu and Huang 2006; Bai et al. 2010). Tolerance (TOL) and variance inflation factor (VIF) are two important indexes for multicollinearity diagnosis. Tolerance smaller than 0.2 is an indicator for the presence of a multicollinearity problem and if it is smaller than 0.1, then there is serious multicollinerarity between independent variables (Menard 1995).

In this study, all the tolerance values are ≥ 0.55 (Table 5) showing that there is no multicollinearity problem among independent landslide factors. Variance inflation factor, which is the reciprocal of tolerance index, is another criterion. Allison (2001) excluded those independent factors from logistic regression analysis if their VIF > 2 and TOL < 0.4. However, no independent landslide factor was excluded from analysis in this study as all factors are not affected by multicollinearity problem. Hosmer-Lemshow test showed that the goodness of fit of an equation can be accepted if the significance of Chi-square is greater than 0.05 (Table 5). Hence, the logistic regression equation that was obtained from SPSS analysis can be expressed as follows.

$$Z = 10.825_{*\text{Distance from river}} + 6.961*\text{Slope} + 6.955*\text{Aspect} + 6.381*\text{Distance from fault} + 6.194*\text{Plan curvature} + 6.08*\text{Rainfall} + 4.823*\text{Lithology} + 3.242*\text{Land use} - 1.947*\text{Profile curvature} - 6.021 \quad \text{..... (13)}$$

From this, it can be implied that distance from river, slope, aspect, distance from fault, plane curvature, rainfall, lithology with positive coefficients in their decreasing order decreasing of importance to cause landslides (Table 5). The landslide susceptibility map was found by substituting the above value of Z in equation 7 and then the map was classified into five susceptibility classes (Figure 9b). Relative operating characteristics (ROC) Curves were used to compare the presence or absence of landslides with the landslide susceptibility map. The ROC values ranges from 0.5 to 1, where 1 indicates a perfect fit and 0.5 represents a random fit (Ayalew and Yamagishi, 2005).

In this study, the entire landslide data was used as a training dataset and a success rate was obtained by comparing these training landslides with the landslide susceptibility map (Bui et al. 2012). The result shows an area under the curve (AUC) value of 0.868 with a succes rate of 86.8%.

6.3 Weights of Evidence (WoE)

After the positive weights(W^+), negative weights(W^-) and weights of contrast values(C) are calculated(Table 2) for each factor's classes through the weights of evidence modelling using ArcGIS 10 and Microsoft excel softwares, assigning the negative and decimal weights of contrast values in ArcGIS is another challenge which has to be tackled systematically

by transforming all the negative contrast values into positive integers by addition and multiplication in Microsoft excel and then back to the real values through arithmetic subtraction and division of raster maps in raster calculator of ArcGIS 10.

The landslide factors with positive weights of contrast values (C) favoring landslide occurrence include slope classes (between 20˚ & 43˚) , aspect classes of N & S orientations, concave and convex plan & profile curvatures, distance from fault (0 - 500 m), land use (barren land), lithology (Melange Matrix & Muddy Turbidite units) and annual rainfall classes between 2950 and 3525 mm.The limitation of othe weights of evidence modelling is its overestimation of the weights of contrast values in case of factor classes with smaller areas as the number of non-landslide pixels in these classes will be smaller.

In order to check the dependency of factors among each other and with respect to landslides, the correlation matrix (Table 5) of landslide factors was prepared using logistic regression model. This test showed that all the nine landslide factors were not correlated with each other or exhibited a very insignificant correlation. Hence it is possible to combine all the landslide factors (Fig. 6) in order to produce the landslide susceptibility map (Fig. 8c). The prediction accuracy of the weights of evidence model was evaluated by extracting the landslide susceptibility map using landslide and non-landslide points and analyzing them in SPSS statistical software. This will help to construct receiving operational characteristic (ROC) curve and the area under the curve (AUC) value (Fig. 9). The AUC value was found to be 0.884 indicating a prediction accuracy of 88.4%. The weight of evidence method avoids the bias (subjectivity) in weighting the factor classes and it also avoids the use of inter-correlated landslide factors (Regmi et al., 2010). Dahal et al. (2008) recommended the preparation of landslide susceptibility map for each landslide type. However, the current study considers the use of all landslides as the overall susceptibility from all landslides is important for decision making (Regmi et al., 2010).

Table 4 Calculating weights using the weights-of-evidence model.

Factor	Class	npix1	nSlide	nclass	nmap	npix2	npix3	npix4	W +	W -	C
Aspect	0 - 22 ; 337 - 360 (N)	4231	30391	97024	666360	26160	92793	543176	1.219	0.008	**1.211**
	22 - 67 (NE)	3223	30391	74356	666360	27168	71133	564836	0.909	0.007	**0.903**
	67 - 112 (E)	2993	30391	81209	666360	27398	78216	557753	0.827	0.028	**0.799**
	112 - 157 (SE)	3705	30391	80853	666360	26686	77148	558821	1.067	-0.001	**1.067**
	157 - 212 (S)	5545	30391	113022	666360	24846	1E+05	528492	1.541	-0.016	**1.558**
	212 - 247 (SW)	2694	30391	58326	666360	27697	55632	580337	0.711	-0.001	**0.712**
	247 - 292 (W)	4064	30391	80839	666360	26327	76775	559194	1.173	-0.015	**1.187**
	292 - 337 (NW)	3936	30391	80731	666360	26455	76795	559174	1.136	-0.010	**1.146**
Distance from fault (m)	0 - 500	9629	30391	162042	666360	20762	152453	483556	2.273	-0.107	**2.380**
	500 - 1000	7719	30391	136865	666360	22672	129146	506823	1.964	-0.066	**2.030**
	1000 - 1500	5032	30391	104054	666360	25359	99022	536947	1.424	-0.012	**1.435**
	1500 - 2000	3120	30391	76013	666360	27271	72893	563076	0.873	0.013	**0.860**
	2000 - 2500	1395	30391	54841	666360	28996	53446	582523	0.007	0.041	**-0.034**
	2500 - 3000	1127	30391	46704	666360	29264	45577	590392	-0.216	0.037	**-0.252**
	3000 - 3500	668	30391	37865	666360	29723	37197	598772	-0.754	0.038	**-0.792**
	3500 - 4000	610	30391	25115	666360	29781	24505	611464	-0.847	0.019	**-0.866**
	4000 - 4500	454	30391	13202	666360	29937	12748	623221	-1.148	0.005	**-1.153**
	4500 - 5000	388	30391	7127	666360	30003	6739	629230	-1.307	-0.002	**-1.305**
	5000 - 5500	249	30391	2532	666360	30142	2283	633686	-1.755	-0.005	**-1.751**
Distance from river (m)	0 - 100	1755	30391	115661	666360	28636	113906	522063	0.249	0.138	**0.111**
	100 - 200	2934	30391	102258	666360	27457	99324	536645	0.805	0.068	**0.736**
	200 - 300	3432	30391	92563	666360	26959	89131	546838	0.980	0.031	**0.949**
	300 - 400	3683	30391	83098	666360	26708	79415	556554	1.060	0.004	**1.056**
	400 - 500	3869	30391	72855	666360	26522	68986	566983	1.116	-0.021	**1.137**
	500 - 600	4128	30391	61099	666360	26263	56971	578998	1.191	-0.052	**1.243**
	600 - 700	3764	30391	48973	666360	26627	45209	590760	1.085	-0.058	**1.143**
	700 - 800	2721	30391	36263	666360	27670	33542	602427	0.722	-0.040	**0.761**
	800 - 900	1862	30391	23787	666360	28529	21925	614044	0.312	-0.028	**0.340**
	900 - 1000	1191	30391	14040	666360	29200	12849	623120	-0.158	-0.020	**-0.139**
	1000 - 1500	1052	30391	15539	666360	29339	14487	621482	-0.287	-0.012	**-0.275**
	1500 - 2000	0	30391	224	666360	30391	224	635745	0.000	0.000	**-0.0004**
Land use	Dense Forest	9648	30391	575208	666360	20743	565560	70409	2.276	1.819	**0.457**
	Barren land	20743	30391	78500	666360	9648	57757	578212	3.806	-1.052	**4.859**
	Reservoir	0	30391	3187	666360	30391	3187	632782	0.000	0.005	**-0.005**
	Settlement	0	30391	3637	666360	30391	3637	632332	0.000	0.006	**-0.006**
	River	0	30391	5828	666360	30391	5828	630141	0.000	0.009	**-0.009**
Lithology	Melange matrix	12614	30391	250566	666360	17777	237952	398017	2.698	-0.068	**2.765**
	Muddy turbidite	6049	30391	112377	666360	24342	106328	529641	1.649	-0.039	**1.688**
	Water	9	30391	5172	666360	30382	5163	630806	-5.083	0.008	**-5.091**
	Sandy turbidite	4649	30391	135882	666360	25742	131233	504736	1.330	0.065	**1.264**
	Basalt	1989	30391	40895	666360	28402	38906	597063	0.382	-0.005	**0.387**
	Chert	422	30391	14776	666360	29969	14354	621615	-1.222	0.009	**-1.231**
	Turbidite	1336	30391	35583	666360	29055	34247	601722	-0.039	0.010	**-0.049**
	Limestone	1358	30391	9882	666360	29033	8524	627445	-0.021	-0.032	**0.011**
	Sandstone	1630	30391	39379	666360	28761	37749	598220	0.171	0.006	**0.164**
	Schist	76	30391	2041	666360	30315	1965	634004	-2.948	0.001	**-2.948**
	Ultramafic rocks	118	30391	7714	666360	30273	7596	628373	-2.506	0.008	**-2.514**
	Marine sedimentary rocks	72	30391	11997	666360	30319	11925	624044	-3.002	0.017	**-3.018**
	Felsic plutonic rocks	69	30391	96	666360	30322	27	635942	-3.045	-0.002	**-3.042**
Note: npix1 = nslclass, npix2 = nslide - nslclass, npix3 = nclass - nslclass and npix4 = nmap - nslide - nclass + nslclass											

Table 4 (... continued) Calculating weights using the weights-of-evidence model.

Factor	Class	npix1	nSlide	nclass	nmap	npix2	npix3	npix4	W +	W -	C
Plan curvature	**-66382138137 - - 19549408075**	1219	30391	15736	666360	29172	14517	621452	-0.134	-0.018	**-0.116**
	-19549408075 - - 10182862052	4335	30391	68475	666360	26056	64140	571829	1.247	-0.048	**1.295**
	-10182862052 - - 3571182507	7102	30391	136644	666360	23289	129542	506427	1.853	-0.038	**1.892**
	-3571182507 - 2489523742	7916	30391	184216	666360	22475	176300	459669	1.997	0.023	**1.975**
	2489523742 - 8550229991	5709	30391	147853	666360	24682	142144	493825	1.577	0.045	**1.532**
	8550229991 - 16814829423	3132	30391	86120	666360	27259	82988	552981	0.877	0.031	**0.846**
	16814829423 - 63096586240	978	30391	27316	666360	29413	26338	609631	-0.363	0.010	**-0.372**
Profile curvature	**-75791291861 - - 21933473984**	916	30391	17691	666360	29475	16775	619194	-0.430	-0.004	**-0.426**
	-21933473984 - - 11529122803	3209	30391	68432	666360	27182	65223	570746	0.904	-0.003	**0.908**
	-11529122803 - - 4184874911	5884	30391	132659	666360	24507	126775	509194	1.614	0.007	**1.607**
	-4184874911 - 2547352323	7843	30391	180925	666360	22548	173082	462887	1.985	0.019	**1.966**
	2547352323 - 9891600215	7038	30391	156080	666360	23353	149042	486927	1.842	0.004	**1.838**
	9891600215 - 20907972053	4265	30391	88606	666360	26126	84341	551628	1.229	-0.009	**1.237**
	20907972053 - 76601851904	1236	30391	21967	666360	29155	20731	615238	-0.120	-0.008	**-0.111**
Annual rainfall (mm)	**2475 - 2600**	72	30391	14500	666360	30319	14428	621541	-3.002	0.021	**-3.022**
	2950 - 3050	10003	30391	144279	666360	20388	134276	501693	2.329	-0.162	**2.491**
	3325 - 3525	4338	30391	42939	666360	26053	38601	597368	1.248	-0.091	**1.340**
	3750 - 3975	1790	30391	28558	666360	28601	26768	609201	0.270	-0.018	**0.287**
	2325 - 2475	4	30391	3497	666360	30387	3493	632476	-5.894	0.005	**-5.900**
	2700 - 2825	1108	30391	89956	666360	29283	88848	547121	-0.233	0.113	**-0.347**
	2600 - 2700	479	30391	29332	666360	29912	28853	607116	-1.093	0.031	**-1.124**
	2825 - 2950	954	30391	50051	666360	29437	49097	586872	-0.388	0.048	**-0.437**
	3175 - 3325	2372	30391	35212	666360	28019	32840	603129	0.572	-0.028	**0.600**
	3525 - 3750	2888	30391	33821	666360	27503	30933	605036	0.787	-0.050	**0.837**
	3975 - 4216	845	30391	31501	666360	29546	30656	605313	-0.513	0.021	**-0.535**
	3050 - 3175	5538	30391	162714	666360	24853	157176	478793	1.540	0.083	**1.457**
Slope (˚)	**[0 - 12]**	570	30391	41717	666360	29821	41147	594822	-0.916	0.048	**-0.964**
	(12 - 20]	2427	30391	87186	666360	27964	84759	551210	0.597	0.060	**0.537**
	(20 - 26]	4584	30391	115353	666360	25807	110769	525200	1.313	0.028	**1.285**
	(26 - 31]	5631	30391	124866	666360	24760	119235	516734	1.560	0.003	**1.557**
	(31 - 36]	6727	30391	127043	666360	23664	120316	515653	1.783	-0.040	**1.824**
	(36 - 43]	7171	30391	124735	666360	23220	117564	518405	1.866	-0.065	**1.931**
	(43 - 64]	3281	30391	45460	666360	27110	42179	593790	0.929	-0.046	**0.975**
Note: npix1 = nslclass, npix2 = nslide - nslclass, npix3 = nclass - nslclass and npix4 = nmap - nslide - nclass + nslclass											

6.3.1 Test for Conditional Independence in WoE model

The three statistical tests for checking the dependency of factors with respect to landslides are pair wise comparison, principal component analysis and logistic regression (Regmi et al., 2010b). Before combining the weights of different landslide factors, it is important to ascertain that these factors are independent from one another with respect to landslides (Van Westen et al., 2003; Dahal eta al., 2008b). For this purpose logistic regression was applied although the pair wise comparison was preferred by some researchers (Dahal eta al., 2008b; Regmi et al., 2010b). In this study, the raster maps of the weights of contrast (C) values for the nine landslide factors were extracted with landslide and non-landslide points. These were arranged in SPSS statistical software in such a way that landslide with presence (1) and absence (0) and the weight of contrast (C) values of each factor were analyzed using binary logistic regression in order to check the degree of correlation among the landslide factors. Based on this analysis, all the nine landside factors showed

either no or very insignificant correlation (Table 5) suggesting that all the factors are independent from each other. As a result, these factor maps can be used to prepare the landslide susceptibility map by summing all.

Table 5 Logistic Regression Correlation matrix for WoE model.

Landslide Factor	Aspect	Distance from fault	Distance from river	Land use	Lithology	Plan curvature	Profile curvature	Rainfall	Slope
Aspect	1.000	0.015	0.038	0.011	0.006	-0.157	0.011	0.011	-0.008
Distance from fault		1.000	-0.011	0.086	-0.112	0.014	0.005	-0.313	-0.005
Distance from river			1.000	-0.009	-0.037	0.011	0.040	0.007	0.005
Land use				1.000	-0.074	0.034	-0.005	-0.104	0.065
Lithology					1.000	0.005	-0.005	-0.076	-0.037
Plan curvature						1.000	-0.243	-0.005	0.010
Profile curvature							1.000	-0.009	-0.115
Rainfall								1.000	0.008
Slope									1.000

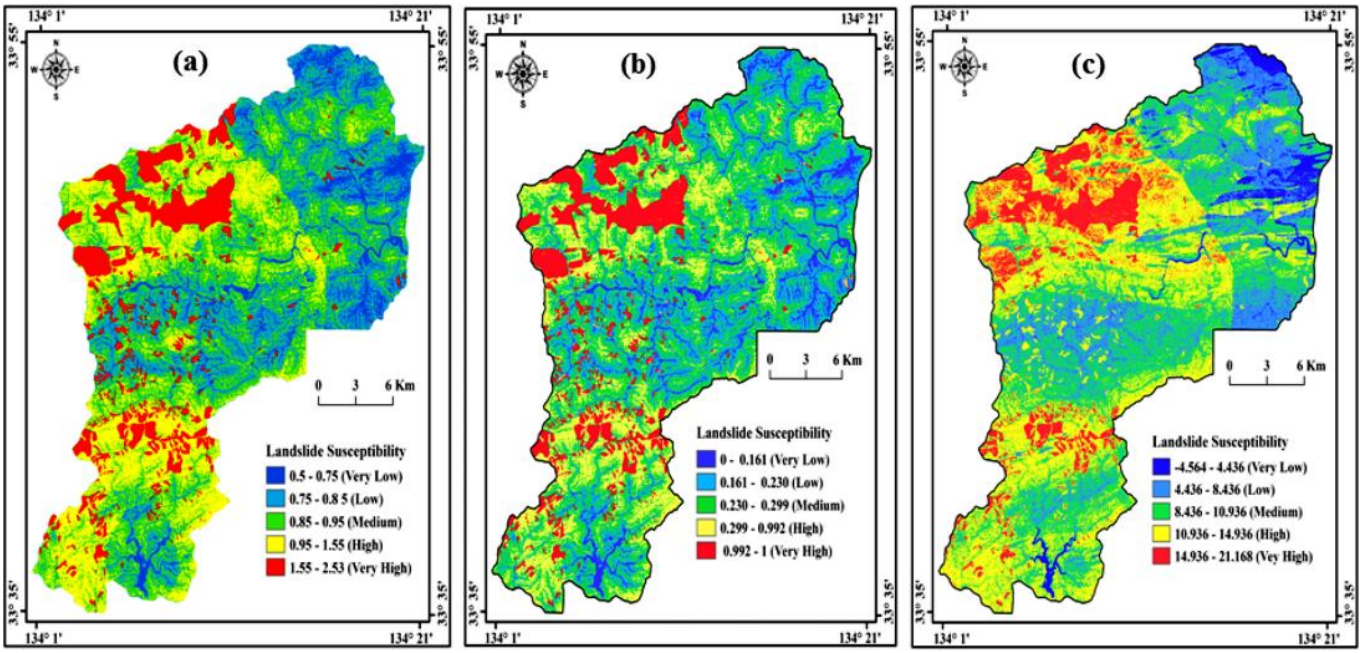

Figure 8 Landslide Susceptibility map of the area using (a) Frequency Ratio Density (b)Logistic Regression and (c) Weights of Evidence models.

6.4 Validation

In the frequency ratio density model, overlying all the landslide inventory data over the final landslide susceptibility map showed that 1%, 2%, 15%, 38% and 44% of the landslides fall in the very low, low, medium, high and very high landslide susceptibility classes respectively. Similarly, in logistic regression model, this overlay operation will provide 1%, 2.5%, 12.5%, 39% and 45% of the landslides to be distributed in the very low, low, medium, high and very high

susceptibility classes respectively. In the weights of evidence model, the landslides used in the analysis were overlaid over the landslide susceptibility map and this showed that 2%, 3%, 17%, 36% and 42% of the landslides fall in the very low, low, medium, high and very high susceptibility classes respectively. All these three validation attempts were also ascertained by the high receiver operating characteristics curve (ROC) values (Fig. 9). The fact that 82%, 84% and 78% of the landslides that fall under the high and very high susceptibility classes of FR density, LR and WoE models respectively showed that these models predict the future probability of landslide occurrence with very good level of accuracy.

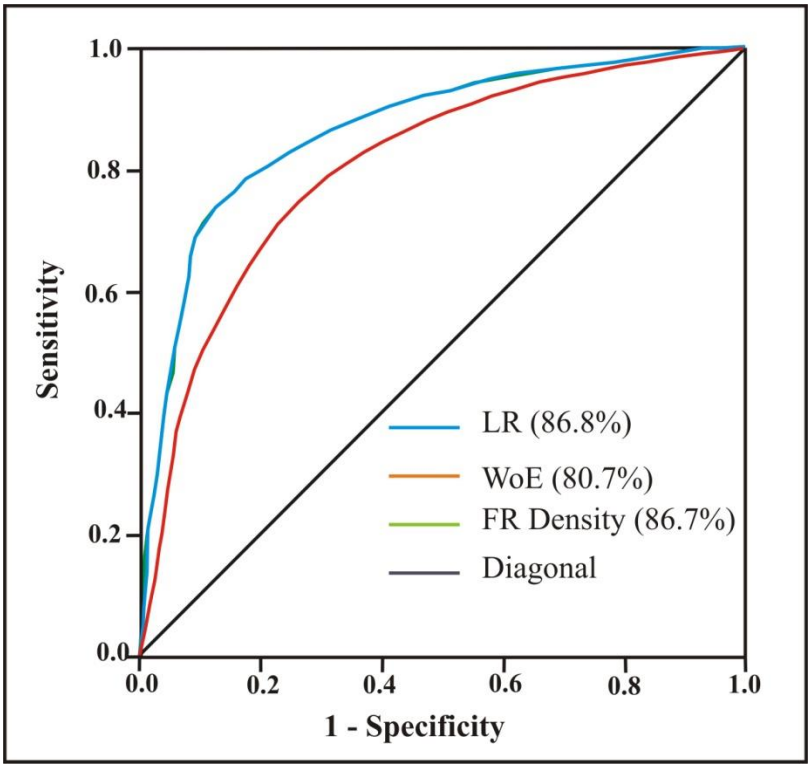

Figure 9 ROC Curve for FR Density, LR (equal landslide and non-landslide points) and Weights of Evidence models.

7. Conclusion

Landslides have inflicted the loss of human lives, properties, road damages and affected the environment in Yanase and Naka Catchments of south east Shikoku, Japan. In order to identify the landslide prone areas for further preventive works and developmental plans, landslide susceptibility mapping should be undertaken. For this purpose, the frequency ratio density, logistic regression and weights of evidence models were applied among the different GIS-based statistical (probabilistic) approaches. The weights of evidence model involves preparing landslide inventory and landslide factors, analyzing and calculating positive and negative weights, the weights of contrast values using ArcGIS 10 and microsoft excel softwares. After transforming the weights of contrast values (C) into positive integers, these values were assigned to each raster map in each factor class for further subtraction and division operations in a raster calculator of ArcGIS so as to get the original weights of contrast values. In weights of evidence modelling, checking the conditional independence of landslide factoors is an important step before adding the raster maps of factors with weights of contrast

values. This was accomplished using logistic regression method which can provide a correlation matrix among landslide factors. This correlation indicates that all of the nine landslide factors didn't show any correlation. This helps to prepare the landslide susceptibility of the area using this model with a reclassification technique based on natural breaks method. However, the reliability of the landslide susceptibility map should be checked for its prediction and validation accuracies. The prediction accuracy, which can be evaluated by the area under the curve (AUC) value, was found to be 80.7%. For validation, landslides used for the analysis were overlaid and this showed that 78 % of the landslides fall in high and very high susceptibility classes.

In case of appliying logistic regression model in this study, it was found that using equal proportion of landslide- and non-landslide points resulted a better prediction accuracy instead of using unequal proportions. The coefficients obtained for distance from river, slope, aspect, distance from fault, plan curvature, rainfall, lithology and land use showed higher positive values with a decreasing trend indicating the highest degree of influence or control in initiating landslide while profile curvature showed negative values indicating the least degree of influence. Choosing an appropriate reclassification technique determines how the resulting landslide susceptibility map looks like and also influences the validation accuracy. In this study, the values in the landslide susceptibility index map are unevenly distributed and as a result the application of natural breaks reclassification mdethod provided a good result unlike other methods.

From the frequency ratio and frequency ratio density models, the frequency ratio values of a certain factor classes that are greater than 1 and density values greater than 0.0458 showed a good correlation with landslide occurrence as can be seen from table 1. Although these two models provide a very close predictive result but still the frequency ratio density model provided a slightly better estimate for landslide susceptibility mapping and assessment (Table 3).

Generally, from the five models that have been utilized to select the best three models, the frequency ratio density, logistic regression with equal proportions of landslides & non-landslides and the weights of evidence were used to generate the landslide susceptibility maps of the study area. Even though the predictive rates through area under the curve (AUC) of the receiver operating characteristics (ROC) curves from these three models showed very close results but still the AUC for logistic regression with equal proportions of landslide- and non-landslide points indicated a slightly greater value. For the validation of landslide susceptibility maps, most of the landslides in the selected susceptibility map fall in the high and very high susceptibility classes which affirmed that the model is quite acceptable.

Acknowledgements

The first author would like to thank Japan's Ministry of Education, Culture, Science and Technology (MEXT) for the scholarship grant to pursue his PhD study from April 3, 2012 up to September 3, 2015. In this time period, the first author has collected some secondary data for analysis from different Japanese Government Organizations. In addition, the Geo-Disaster Research Laboratory in the Department of Civil and Environmental Engineering, Graduate School of Science and Engineering of Ehime University should also be acknowledged for hosting the first author during his PhD study.

Authors' Contributions

MM as a first author, has mostly participated in the whole process including data collection, database preparation, compiling the results and incorporated critical comments from NPB and finalized the draft for journal submission after a consensus is reached with NPB. NPB has participated from the inception and design of this paper and helped greatly in data preparation and analysis. NPB has given the final approval of the version to be published.

Competing Interests

The authors declare that we do not have any financial or non-financial competing interests with any individual or institution.

Authors' Information

Matebie Meten (PhD)[1*]
Department of Geology
College of Applied Sciences,
Addis Ababa Science and Technology University, Ethiopia
Telephone: +251-911899279
P.O.Box: 16417
E-mail: matebe21@gmail.com
Netra Prakash Bhandary, Ph.D. Eng.(Professor) [2]
Department of Environmental Design, Faculty of Collaborative Regional Innovation
Graduate School of Science and Engineering
Ehime University
3 Bunkyo-cho, Matsuyama 790-8577, JAPAN
Tel/Fax: +81 (0)89 927 8566; Cell: +81 (0)90 3785 5836
Email: netra@ehime-u.ac.jp

Funding

No funding was used for this manuscript preparation.

Availability of Data and Materials

All materials that were used for the article compilation were properly cited.

Author Details

The first author is an assistant professor of Engineering Geology at the Department of Geology, College of Applied Sciences in Addis Ababa Science and Technology University. The second author is a Professor of Civil Engineering in the Department of Environmental Design, Faculty of Collaborative Regional Innovation, Graduate School of Science and Engineering at Ehime University.

References

Abella EAC, Van Westen CJ (2008) Qualitative landslide susceptibility assessment by multicriteria analysis: a case study from San Antonio del Sur, Guanta´namo Cuba. Geomorphology 94(2008): 453–466

Akgün A and Bulut F (2007) GIS-based landslide susceptibility for Arsin-Yomra (Trabzon, North Turkey) region. Environ Geol (2007) 51:1377–1387 DOI 10.1007/s00254-006-0435-6

Akgün A, Turk N (2011) Mapping erosion susceptibility by a multivariate statistical method: a case study from the Ayvalik region, NW Turkey. Comput Geosci 37(2011):1515–1524

Alkhasawneh MS, Ngah UK, Tay LT, et al. (2013) Determination of important topographic factors for landslide mapping analysis using MLP Network. Hindawi Publishing Corporation. The Scientific World Journal Volume 2013, Article ID 415023. DOI: 10.1155/2013/415023

Allison PD (2001) Logistic Regression Using the SAS System: Theory and Application. Wiley Interscience, New York, USA. p 28.

Atkinson PM, Massari R (1998) Generalized linear modeling of landslide susceptibility in the Central Apennines. Computers and Geosciences 24(4): 373-385. DOI: 10.1016/S0098-3004 (97)00117-9

Ayalew L, Yamagishi H (2005) The application of GIS-based logistic regression for landslide susceptibility mapping in the Kakuda- Yahiko Mountains, Central Japan. Geomorphology 65(2005): 15–31

Ayalew L, Yamagishi H, Marui H, Kanno T (2005) Landslides in Sado Island of Japan: part II. GIS-based susceptibility mapping with comparisons of results from two methods and verifications. Eng Geol 81(2005):432–445

Ayalew L, Yamagishi H, Ugawa N (2004) Landslide susceptibility mapping using GIS-based weighted linear combination, the case in Tsugawa area of Agano River, Niigata Prefecture, Japan. Landslides 1:73–81. doi:10.1007/s10346-003-0006-9

Ayenew T, Barbieri G (2005) Inventory of landslides and susceptibility mapping in the Dessie area, northern Ethiopia. Eng Geol 77(2005):1–15

Bai SB, Wang J, Lv GN, et al. (2010) GIS-based logistic regression for landslide susceptibility mapping of the Zhongxian segment in the Three Gorges area, China. Geomorphology 115: 23-31. DOI: 10.1016/j.geomorph.2009.09.025

Bonham-Carter, G.F. (1994). Geographic information system for geoscientists, modelling with GIS.*Pergamon Press, Oxford, pp 398.*

Bonham-Carter, G.F., 2002. Geographic information systems for geoscientist: modelling with GIS. In: Merriam, D.F. (Ed.), Computer Methods in the Geosciences. Pergamon/Elsevier, New York, pp. 302–334.

Bonham-Carter, G.F., Agterberg, F.P., Wright, D.F.(1988).Integration of geological datasets for gold exploration in Nova-Scotia. Photogrammetric Engineering and Remote Sensing 54, 1585–1592.

Bui DT, Pradhan B, Lofman O (2012) Landslide susceptibility assessment at Hoa Binh Province of Vietnam using Frequency Ratio Model. In: Proceedings of the 2012 Asia Pacific Conference on Environmental Science and Technology Advances in Biomedical Engineering (APEST 2012) held in Kuala Lumpur, Malaysia, 1-2 February 2012. Vol.6, pp 476-484.

Carson MA, Kirkby MJ (1972) Hillslope form and process. Cambridge University Press, London 475 pp

Cervi F, Berti M, Borgatti L, Ronchetti F, Manenti F, Corsini A (2010) Comparing predictive capability of statistical and deterministic methods for landslide susceptibility mapping: a case study in the northern Apennines (Reggio Emilia Province, Italy).Landslides 7:433–444. doi:10.1007/s10346-010-0207-y

Chung CJ (2006) Using likelihood ratio functions for modeling the conditional probability of occurrence of future landslides for risk assessment. Comput Geosci 32(2006):1052–1068

Clerici A, Perego S, Tellini C, Vescovi P (2006) A GIS-based automated procedure for landslide susceptibility mapping by the conditional analysis method: the Baganza valley case study (Italian Northern Apennines). Environ Geol 50:941–961. doi:10.1007/s00254-006-0264-7

Cruden DM, Varnes DJ (1996) Landslide types and processes. In: Turner A.K. and Schuster R.L. (Eds), Landslides: Investigation and Mitigation. Sp. Rep.247, Transportation Research Board, National Research Council, National Academy Press, Washington D.C., pp 36-75

Dahal R.K.*, Hasegawa S.,* Yamanaka M., Nishino K. (2006) Rainfall triggered flow-like landslides: Understanding from southern hills of Kathmandu, Nepal and Northern Shikoku, Japan; IAEG2006 Paper number 819.

Dahal R.K.*, Hasegawa S., Yamanaka M.,, Nonomura A.,(2008a)* Typhoon Rainfall and Landsliding in the Pacific Ocean Side of Japan. *Proceedings of the Eighteenth (2008) International Offshore and Polar Engineering Conference Vancouver, BC, Canada, July 6-11, 2008*

Dahal RK, Hasegawa S, Nonomura A, Yamanaka M, Dhakal S, Paudyal P (2008b) Predictive modeling of rainfall-induced landslide hazard in the Lesser Himalaya of Nepal based on weights-of-evidence. Geomorphology 102(2008):496–510

Dai FC, Lee CF (2002) Landslide characteristics and slope instability modeling using GIS, Lantau Island, Hong Kong. Geomorphology 42(3-4): 213-228. DOI: 10.1016/ S0169-555X (01)00087-3 Geographic Information Technology Training Alliance (GITTA, 2011) Classification of data.

Ercanoglu M, Gokceoglu C (2002) Assessment of landslide susceptibility for a landslide-prone area (north of Yenice, NW Turkey) by fuzzy approach. Environ Geol 41:720–730, doi:10.1007/s00254-001-0454-2

Fell R, Corominas J, Bonnard C, Cascini L, Leroi E, Savage WZ (2008) Guidelines for landslide susceptibility, hazard and risk zoning for land use planning. Eng Geol 102(2008):85–98

Gerscovich DMS, Vargas EA, De Campos TMP (2006) On the evaluation of unsaturated flow in a natural slope in Rio de Janeiro, Brazil. Eng Geol 88(2006):23–40

Guzzetti F, Carrara A, Cardinali M (1999) Landslide hazard evaluation: a review of current techniques and their application in a multi-scale study, central Italy. Geomorphology 31(1-4): 181-216. DOI: 10.1016/S0169-555X (99)00078-1

Guzzetti, F., Mondini A. C., Cardinali, M., Fiorucci F., Santangelo M., ChangM K.T., (2012) Landslide inventory maps: New tools for an old problem. Earth-Science Reviews 112 (2012) 42–66. Elsevier

Hong Y., Hiura H., Shino K., Sassa K., Suemine A., Fukuoka H., Wang G.,(2005) The influence of intense rainfall on the activity of large-scale crystalline schist landslides in Shikoku Island, Japan Landslides (2005) 2:97–105 DOI 10.1007/s10346-004-0043-z

Lee S (2005) Application of logistic regression model and its validation for landslide susceptibility mapping using GIS and remote sensing data. International Journal of Remote Sensing 26(7): 1477-1491. DOI: 10.1080/01431160412331331012

Lee S, Choi J, Woo I (2004) The effect of spatial resolution on the accuracy of landslide susceptibility mapping: a case study in Boun Korea. Geosci J 8(1):51–60

Lee S, Ryu JH, Kim LS (2007) Landslide susceptibility analysis and its verification using likelihood ratio, logistic regression and artificial neural network models: case study of Youngin, Korea. Landslides 4(4): 327-338. DOI: 10.1007/s10346-007- 0088-x

Lee S, Sambath T (2006) Landslide susceptibility mapping in the Damrei Romel area, Cambodia using frequency ratio and logistic regression models. Environ Geol 50:847–855, doi:10.1007/s00254-006-0256-7

Menard S (1995) Applied logistic regression analysis. Sage University Paper Series on Quantitative Applications in Social Sciences, 106. Thousand Oaks, California, USA. p 98.

Meten M, Bhandary NP, Yatabe R (2015a): Effect of landslide factor combinations on the prediction accuracy of landslide susceptibility maps in the Blue Nile Gorge of Central Ethiopia. Meten et al. Geoenvironmental Disasters (2015) 2:9 DOI 10.1186/s 40677-015- 0016-7.

Meten M, Bhandary NP, Yatabe R (2015b): GIS-based landslide susceptibility Modelling of Debre Sina area in Central Ethiopia. Journal of Mountain Science. Accepted on Sept 6, 2015). Published online on November 18, 2015

Ohlamacher GC (2007) Plan curvature and landslide probability in regions dominated by earth flows and earth slides. Eng Geol 91(2007):117–134

Ohlmacher GC, Davis JC (2003) Using multiple logistic regression and GIS technology to predict landslide hazard in northeast Kansas, USA. Eng Geol 69(2003):331–343

Pradhan B (2010) Landslide Susceptibility mapping of a catchment area using frequency ratio, fuzzy logic and multivariate logistic regression approaches. Journal of the Indian Society of Remote Sensing 38(2): 301-320.

Pradhan B, Lee S, Buchroithner MF (2010) A GIS-based backpropagation neural network model and its cross-application and validation for landslide susceptibility analyses. Comput Environ Urban Syst 34(2010):216–235

Regmi AD, Devkota KC, Yoshida K, et al. (2014) Application of frequency ratio, statistical index, and weights-of-evidence models and their comparison in landslide susceptibility mapping in Central Nepal Himalaya. Arabian Journal of Geosciences 7(2): 725-742 DOI: 10.1007/s12517-012-0807-z

Regmi NR, Giardino JR, Vitek JD (2010a) Assessing susceptibility to landslides: using models to understand observed changes in slopes. Geomorphology 122(2010):25–38

Regmi, N.R., Giardino J.R. andVitek J.D. (2010b).Modeling susceptibility to landslides using the weights of evidence approach: Western Colorado, USA. Geomorphology 115 (2010)172-187.

Ruff M, Czurda K (2008) Landslide susceptibility analysis with a heuristic approach in the Eastern Alps (Vorarlberg, Austria). Geomorphology 94(2008):314–324

Saha AK, Gupta RP, Sarkar I, Arora MK, Csaplovics E (2005) An approach for GIS-based statistical landslide susceptibility zonation—with a case study in the Himalayas. Landslides 2:61–69. doi:10.1007/s10346-004-0039-8

Schicker R, Moon V (2012) Comparison of bivariate and multivariate statistical approaches in landslide susceptibility mapping at a regional scale. Geomorphology 161-162: 40-57. DOI: 10.1016/j.geomorph.2012.03.036

Shahabi H, Khezri S, Ahmad BB, et al. (2014) Landslide susceptibility mapping at central Zab basin, Iran: A comparison between analytical hierarchy process, frequency ratio and logistic regression models. Catena 115: 55-70. DOI: 10.1016/j.catena.2013.11.014

Sharma M., Kumar R. (2008) GIS- based landslide hazard zonation: a case study from the Parwanoo area, Lesser and outer Himalaya, H.P., India. Bull EngGeol Environ (2008) 67:129-137. DOI 10.1007/s 10064-007-0113-2.

Terlien MTJ, Van Westen CJ, Van Asch TWJ (1995) Deterministic modelling in GIS based landslide hazard assessment. In: Carrara A, Guzzetti F (eds) Geographical information system in assessing natural hazard. Kluwer Academic Publishers, Dordrecht, pp 57–78

Thiery Y, Malet JP, Sterlacchini S, Puissant A, Maquaire O (2007) Landslide susceptibility assessment by bivariate methods at large scales: application to a complex mountainous environment. Geomorphology 92(2007):38–59

Van Westen CJ (2002) Use of weights of evidence modeling for landslide susceptibility mapping. International Institute for Geoinformation Science and Earth Observation (ITC), Enschede, The Netherlands.

Van Westen CJ, Rengers N, Soeters R (2003). Use of geomorphological information inindirect landslide susceptibility assessment. Natural Hazards 30, 399–419.

Wan S (2009) A spatial decision support system for extracting the core factors and thresholds for landslide susceptibility map. Eng Geol 108(2009):237–251

Wang G, Suemine A, Furyua G, Kaibori M.,Sassa K.(2006) Rainstorm-induced landslides in Kisawa village, Tokushima Prefecture, Japan. *IAEG2006 Paper number 16* © The Geological Society of London 2006*7*

Wang G, Suemine A, Schulz WH (2010) Shear-rate-dependent strength control on the dynamics of rainfall triggered landslides,Tokushima Prefecture, Japan EARTH SURFACE PROCESSES AND LANDFORMS *Earth Surf. Process. Landforms* (2010) (www.interscience.wiley.com) DOI: 10.1002/esp.1937

Wilson JP, Gallant JC (2000) Terrain analysis principles and applications. Wiley, New York, USA.

Yalcin A, Reis S, Aydinoglu A (2011) A GIS-based comparative study of frequency ratio, analytical hierarchy process, bivariate statistics and logistic regression methods for landslide susceptibility mapping in Trabzon, NE Turkey. Catena 85(3): 274-287. DOI: 10.1016/j.catena.2011.01.014

Yesilnacar E, Topal T (2005) Landslide susceptibility mapping: a comparison of logistic regression and neural networks methods in a medium scale study, Hendek region (Turkey). Engineering Geology 79(3-4): 251-266. DOI: 10.1016/j.enggeo. 2005.02.002

Yilmaz I, Keskin I (2009) GIS based statistical and physical approaches to landslide susceptibility mapping (Sebinkarahisar, Turkey). Bull EngGeol Environ 68:459–471. doi:10.1007/s10064-009-0188-z

Zhu L, Huang J (2006) GIS-based logistic regression method for landslide susceptibility mapping in regional scale. J Zhejiang Univ Sci A 7(12):2007–2017

http://www.data.jma.go.jp/gmd/risk/obsdl/index.php

www.gsj.jp/Map/EN/dgm.htm

Figures

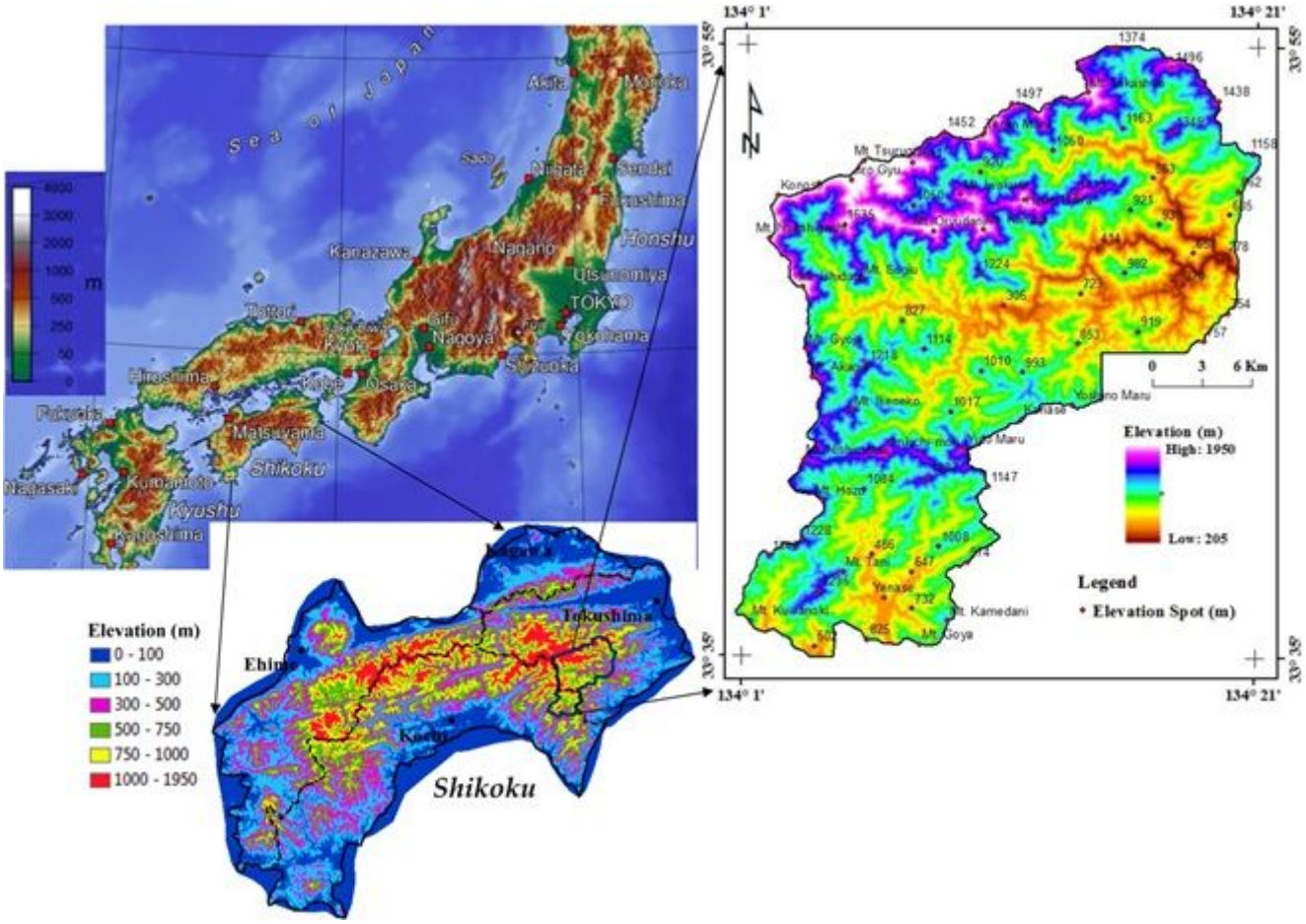

Figure 1

Location map of the study area.

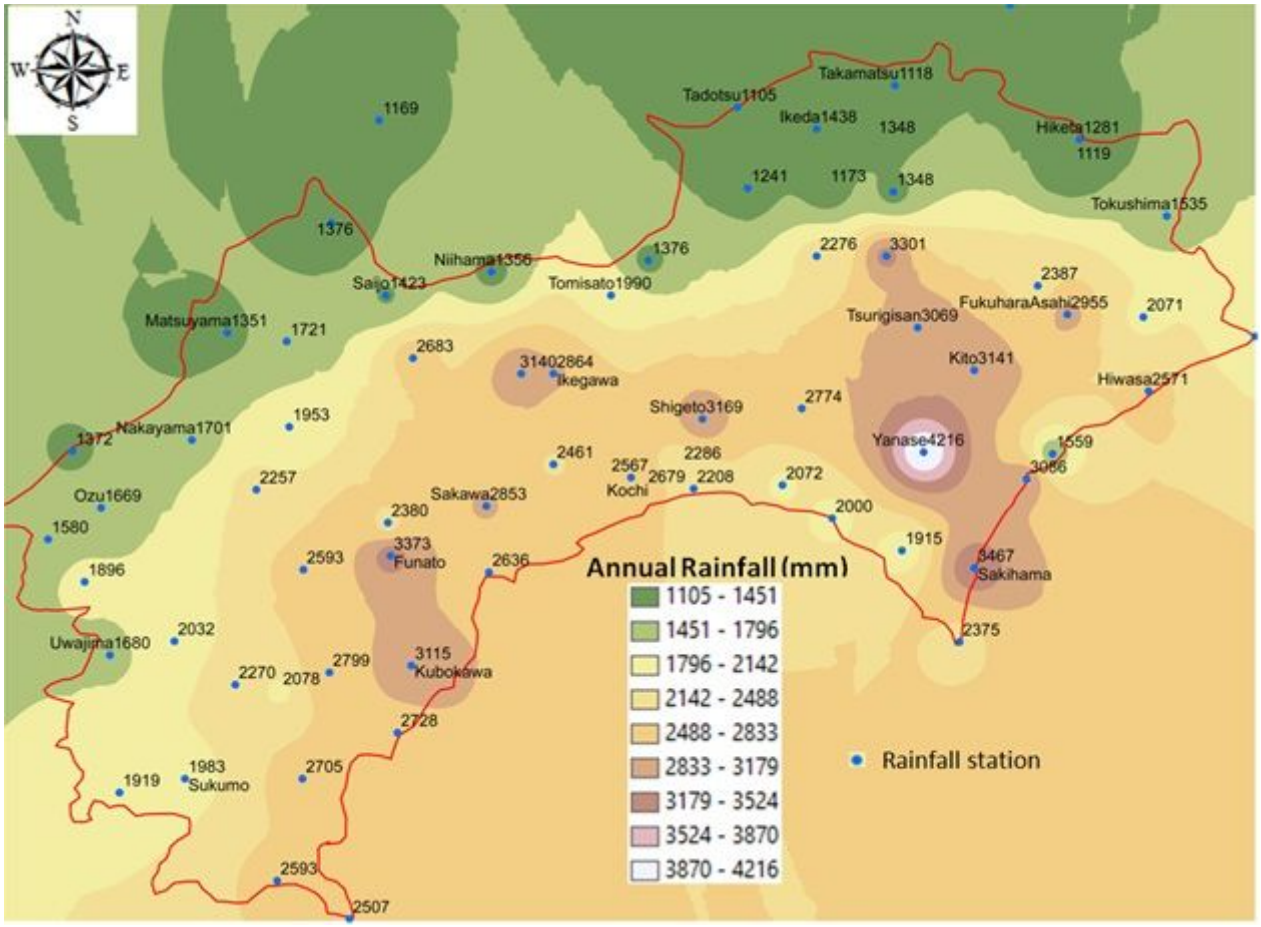

Figure 2

Thirty years average annual rainfall of Shikoku Island.

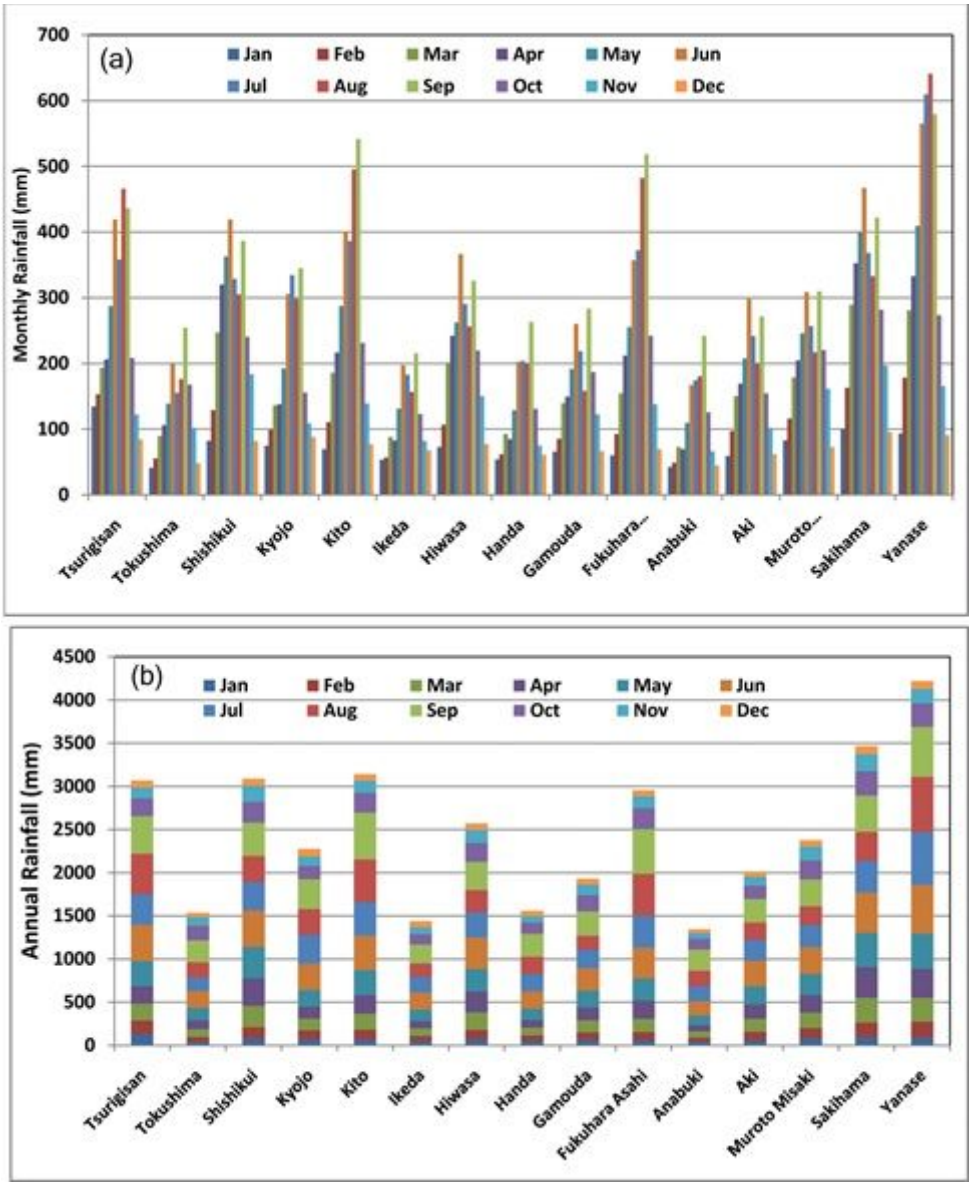

Figure 3

Thirty year's average rainfall (1985 - 2014) showing (a) Monthly rainfall (b) Annual rainfall of the study area.

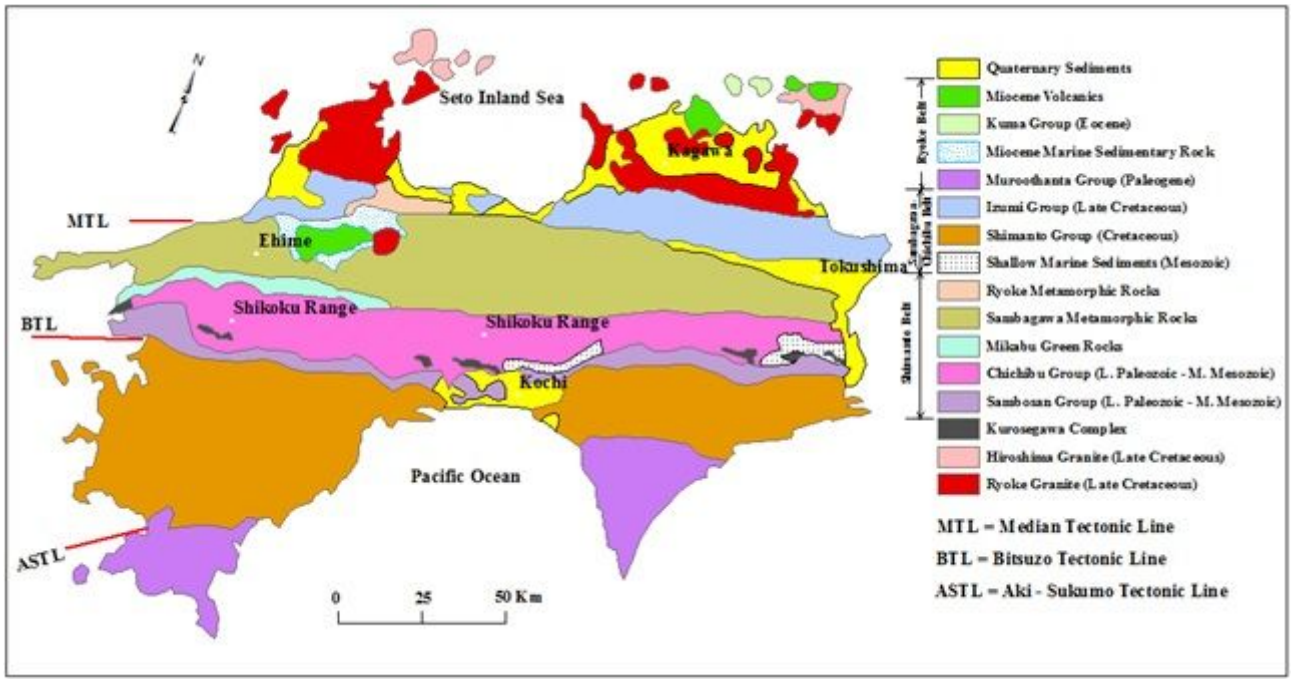

Figure 4

Simplified geological map of Shikoku Island (modified after Dahal et al. 2006)

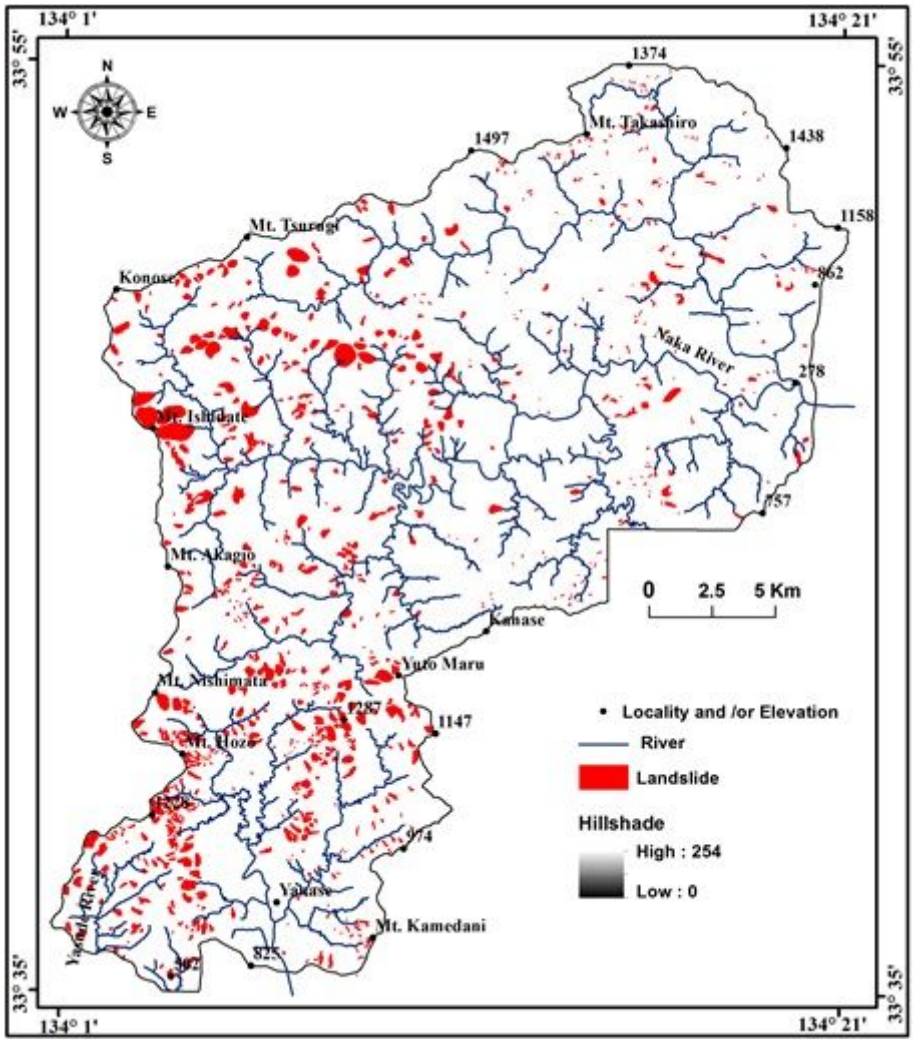

Figure 5

Landslide inventory map with river networks.

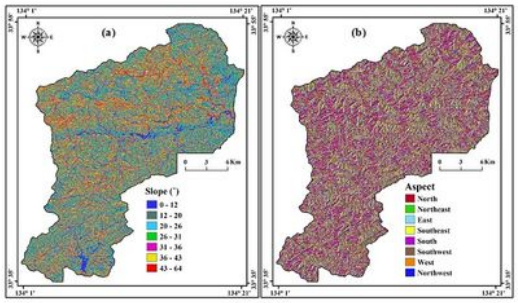

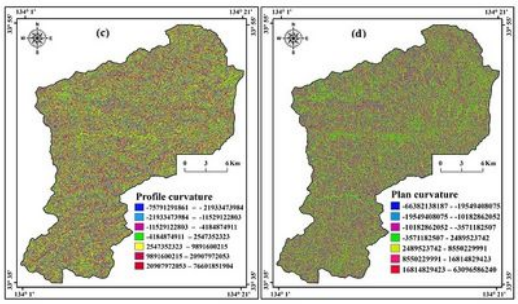

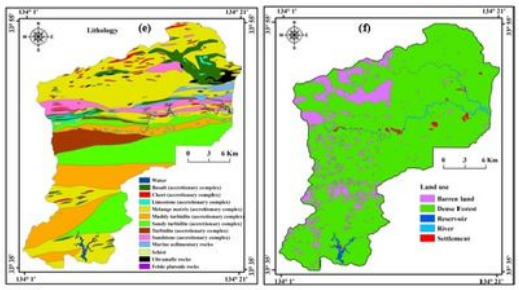

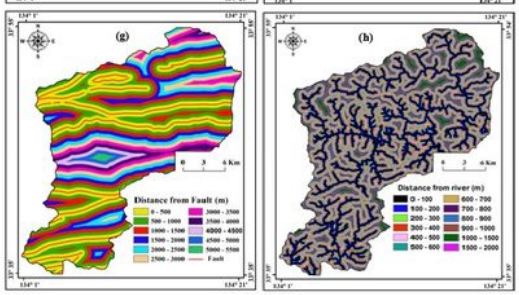

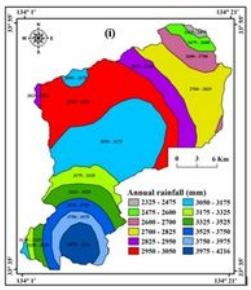

Figure 6

Landslide Factors (a) Slope (b) Aspect (c) Profile curvature (d) Plan curvature (e) Lithology (f) Land use (g) Distance from fault (h) Distance from river (i) Annual rainfall.

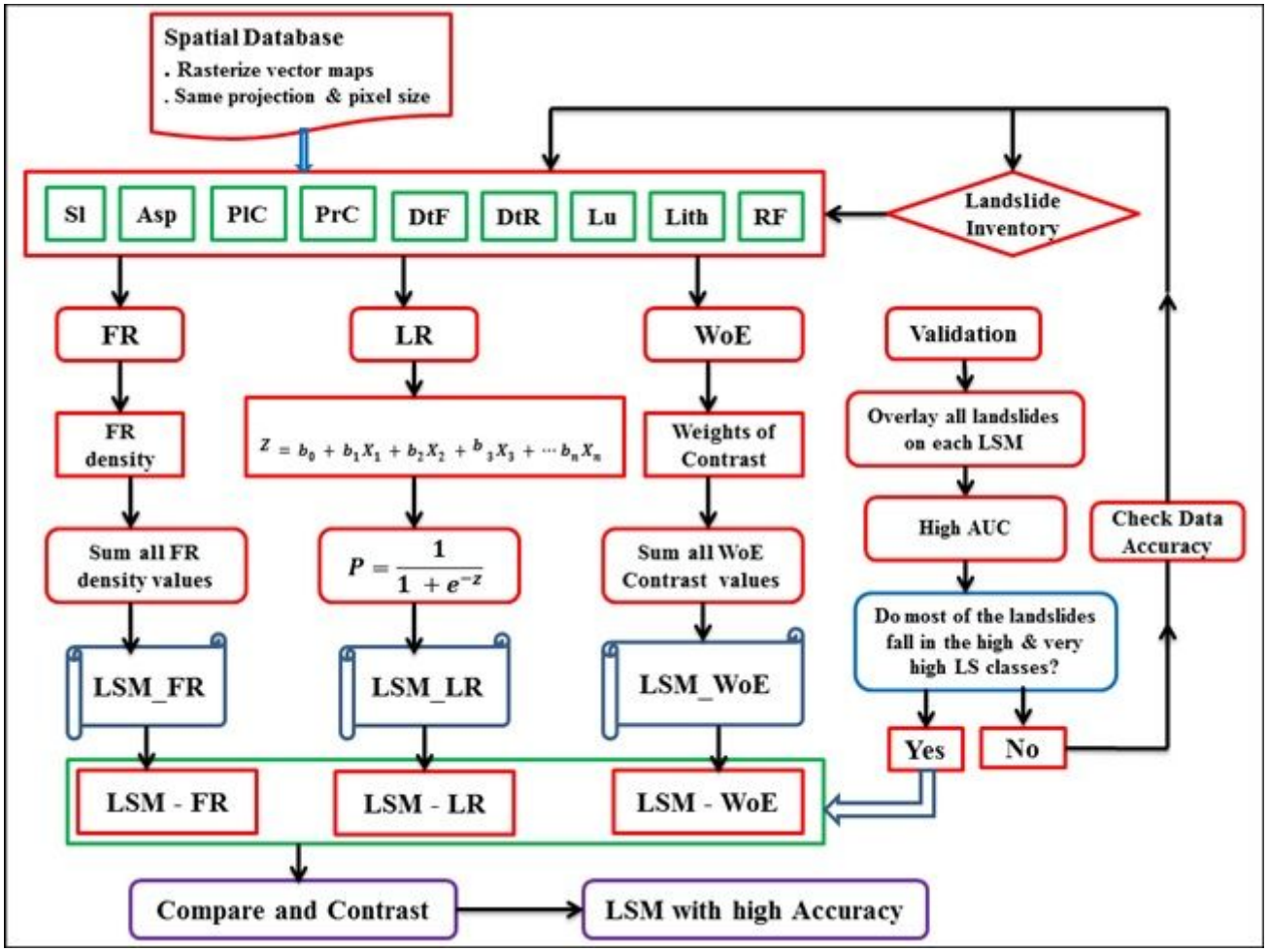

Figure 7

Flow chart of the work(Sl = slope, Asp = aspect, Prc = profile curvature, Plc = plan curvature, Lith = lithology, DtF = distance to fault, DtR = distance to river, Lu = landuse, AR = Annual Rainfall, FR =Frequency Ratio,LR = Logistic Regression, WoE =Weights of Evidene and LS = Landslide Susceptibility, LSM =Landslide Susceptibility Map and AUC = Area Under the curve).

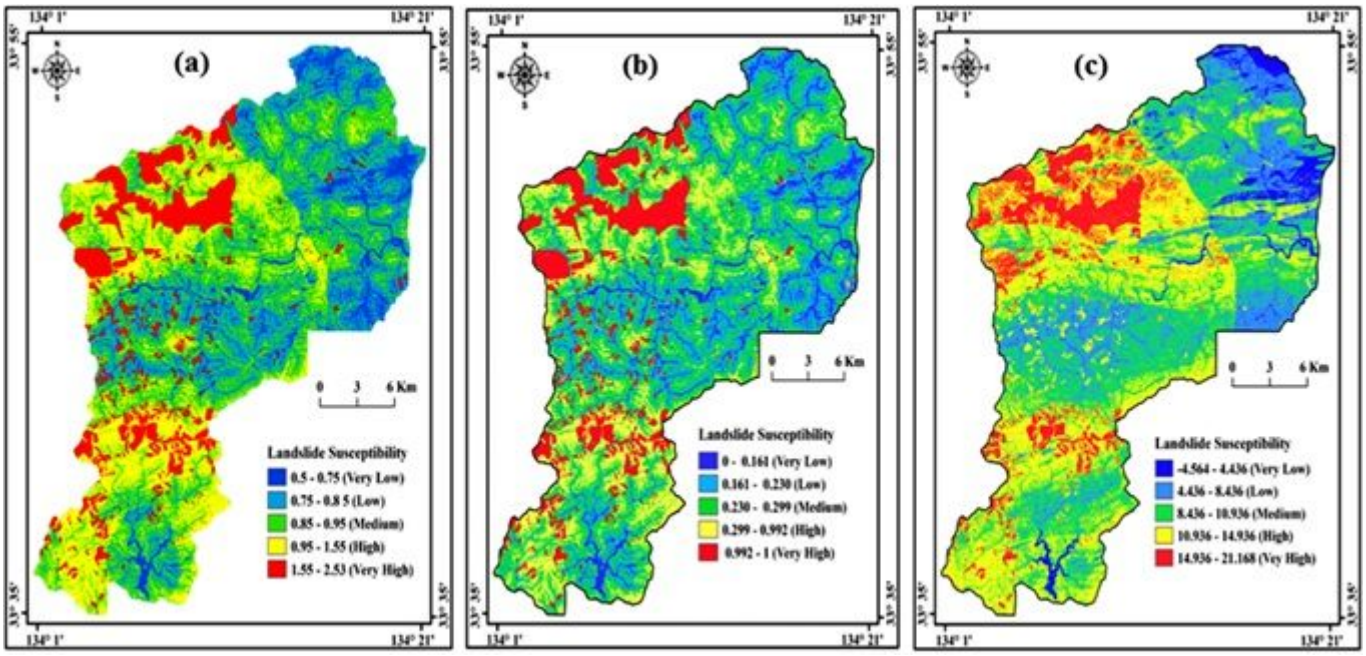

Figure 8

Landslide Susceptibility map of the area using (a) Frequency Ratio Density (b)Logistic Regression and (c) Weights of Evidence models.

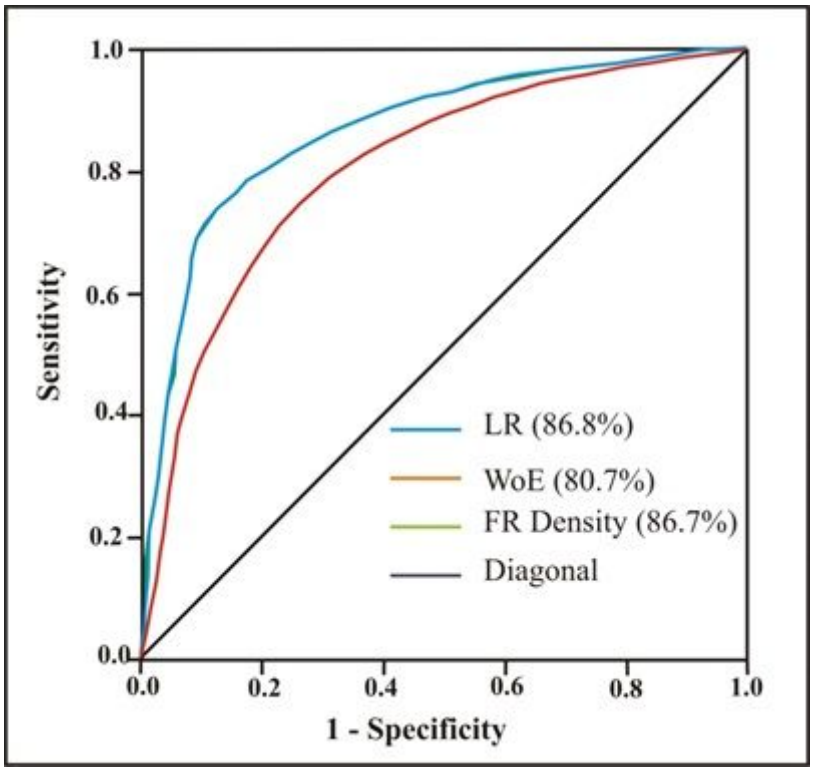

Figure 9

ROC Curve for FR Density, LR (equal landslide and non-landslide points) and Weights of Evidence models.